Catchment hydrological responses to forest harvest amount and spatial pattern

Alex Abdelnour,[1] Marc Stieglitz,[1,2] Feifei Pan,[1,3] and Robert McKane[4]

Received 26 October 2010; revised 17 July 2011; accepted 25 July 2011; published 27 September 2011.

[1] Forest harvest effects on streamflow generation have been well described experimentally, but a clear understanding of process-level hydrological controls can be difficult to ascertain from data alone. We apply a new model, Visualizing Ecosystems for Land Management Assessments (VELMA), to elucidate how hillslope and catchment-scale processes control stream discharge in a small Pacific Northwest catchment. VELMA is a spatially distributed ecohydrology model that links hydrological and biogeochemical processes within watersheds. The study site is WS10 of the H.J. Andrews LTER, a 10 ha forested catchment clearcut in 1975. Simulated and observed daily streamflow are in good agreement for both the pre- (1969–1974) and postharvest (1975–2008) periods (Nash-Sutcliffe efficiency = 0.807 and 0.819, respectively). One hundred scenarios, where harvest amounts ranged from 2% to 100% were conducted. Results show that (1) for the case of a 100% clearcut, stream discharge initially increased by ~29% or 345 mm but returned to preclearcut levels within 50 years, and (2) annual streamflow increased at a near linear rate of 3.5 mm year^{-1} for each percent of catchment harvested, irrespective of location. Thereafter, to assess the impact of harvest location on stream discharge, 20 harvest scenarios were simulated, where harvest amount was fixed at 20% but harvest location varied. Results show that the streamflow response is strongly sensitive to harvest distance from the stream channel. Specifically, a 20% clearcut area near the catchment divide resulted in an average annual streamflow increase of 53 mm, whereas a 20% clearcut near the stream resulted in an average annual streamflow increase of 92 mm.

Citation: Abdelnour, A., M. Stieglitz, F. Pan, and R. McKane (2011), Catchment hydrological responses to forest harvest amount and spatial pattern, *Water Resour. Res., 47*, W09521, doi:10.1029/2010WR010165.

1. Introduction

[2] Forest harvest effects on streamflow dynamics have been well described experimentally [*Beschta et al.*, 2000; *Bowling et al.*, 2000]. For example, results from paired-catchment studies have shown that (1) removal of forest cover increases water yield [*Hibbert*, 1966; *Keppeler and Ziemer*, 1990; *Rothacher*, 1970] and peak streamflow [*Golding*, 1987; *Harr and McCorison*, 1979; *Jones*, 2000; *Jones and Grant*, 1996] by decreasing evapotranspiration [*Bosch and Hewlett*, 1982]; (2) regrowth after harvest decreases water yield [*Jones*, 2000; *Jones and Post*, 2004; *Sahin and Hall*, 1996]; and (3) the initial response to harvest and the subsequent recovery of annual, peak, and low flows are highly variable and difficult to predict [e.g., *Bosch and Hewlett*, 1982; *Hibbert*, 1966; *Jones and Post*, 2004; *Stednick*, 1996].

[3] The factors that control the variability in streamflow response to harvest include harvest amount, vegetation type, and climatic/hydrologic regimes. *Stednick*'s [1996] meta-analysis of 95 paired-catchment studies highlighted major differences in the response of annual streamflow to harvest across eight climate regions within the United States. At the two extremes, catchments in the Rockies and the Pacific Coast yielded 9 and 50 mm more streamflow annually for every 10% increase in harvest area, respectively (below 15% and 25% clearcut, respectively, there was no discernable increase in streamflow for either region). Moreover, *Stednick*'s [1996] analysis showed a large variability in the relationship between harvest amount and annual water yield within each of the eight climate regions. For example, the increase in annual water yield following a 100% clearcut in Rocky mountain watersheds ranged from 0 to over 350 mm. It was also unclear how harvest location within a watershed, as opposed to harvest amount, impacted stream response [*Stednick*, 1996].

[4] Analyses that have focused on ecohydrological controls have provided important insights into the variability of streamflow responses to harvest. *Jones* [2000] and *Jones and Post* [2004] analyzed paired coniferous forest catchments in the Pacific Northwest and northeastern United States and found that the magnitude, seasonality, and duration of streamflow responses to forest harvest and regrowth were consistent with fundamental water balance concepts

[1]Department of Civil and Environmental Engineering, Georgia Institute of Technology, Atlanta, Georgia, USA.
[2]School of Earth Atmospheric Sciences, Georgia Institute of Technology, Atlanta, Georgia, USA.
[3]Department of Geography, University of North Texas, Denton, Texas, USA.
[4]U.S. Environmental Protection Agency, Corvallis, Oregon, USA.

0043-1397/11/2010WR010165

in hydrology. Specifically, *Jones* [2000] found that peak discharge in 10 experimental watersheds in the western Cascade Range of Oregon increased by as much as 50% for a 100% clearcut, by as much as 30% for a 50% clearcut, and by as much as 20% for a 25% clearcut. *Jones and Post* [2004] examined the seasonality of streamflow to forest clearcut and found that the relative increase in streamflow is highest during warm and dry seasons when evapotranspiration is high, and the absolute increase in streamflow is largest in moist seasons when evapotranspiration is low. Nonetheless, although carefully designed paired-catchment experiments and statistical analyses can provide strong circumstantial evidence for process-level controls, they cannot be used alone to quantify the contribution of specific processes to observed streamflow responses.

[5] Process-based simulation models can address this need by providing a framework for synthesizing data describing catchment responses to climate, harvest, and other disturbances. When properly constrained, models allow a self-consistent representation and analysis of process-level interactions within catchments, as well as the ability to isolate the contribution of specific processes to observed responses. Models can also extend a data set by allowing behavior of unmeasured system components to be examined. Similarly, models can be used to isolate the effect of a "target" treatment factor from the effects of other factors that may be unavoidably altered within a single treatment [*McKane et al.*, 1997]. These properties are apparent in various modeling analyses of experimental data for paired-catchment studies in the Pacific Northwest. For example, *Tague and Band* [2000] used the RHESSys ecohydrological model to isolate the effects of harvest and roads on streamflow. *Waichler et al.* [2005] applied the dynamic hydrology soil vegetation model (DHSVM) [*Wigmosta et al.*, 1994] to three watersheds in the H.J. Andrews Experimental Forest in order to quantify the effects of forest harvest, without roads, on streamflow, peakflow, and water balance. *Whitaker et al.* [2002] used the DHSVM hydrological model to evaluate peak flow sensitivity to clearcut at various elevation bands in a snow-dominated catchment in British Columbia. *Sayama and McDonnell* [2009] used the OHDIS-KWMSS [*Tachikawa et al.*, 2004] hydrological model to infer the age and upland source areas of water contributing to streamflow. Thus, models such as these can provide a more detailed and process-based understanding of experimental responses that would be impossible with the data alone.

[6] However, existing process-based models have some disadvantages. Many models are too simple to simulate process-level controls of interest—e.g., interactions among hydrological and ecological processes. At the other extreme, some models are so complex that they require calibration and forcing data that are often unavailable. Finally, some models are too computationally expensive to simulate large watersheds and landscapes, and require a high level of expertise to implement. Moreover, for a variety of reasons, most current modeling frameworks have been limited to the research community [*Beckers et al.*, 2009]. Therefore, we contend that there is a need for a balanced approach; specifically, an accessible, spatially distributed, ecohydrological model that is both computationally efficient and relatively easy to implement for analyzing the effects of changes in climate, land use, and land cover, on watershed processes at scales relevant to formulating management decisions.

[7] We present a relatively simple ecohydrological model that aims to address both scientific and decision making needs. We apply this model to a small experimental catchment in the Pacific Northwest to investigate the ecohydrological controls on: (1) the effects of clearcut on stream discharge, soil moisture, and evapotranspiration, (2) the relation between harvest amount and catchment hydrological response, (3) the sensitivity of streamflow to harvest location, and (4) threshold behavior in the catchment hydrological response.

[8] A description of the study area and history is provided in section 2. An overview of the ecohydrological model VELMA is provided in section 3. Simulations methods and model calibration are described in section 4. Simulations results are described in section 5. Discussion and conclusion are presented in sections 6 and 7, respectively.

2. Site Description

[9] Watershed 10 (WS10) of the H.J. Andrews Experimental Forest (HJA) is a small 10.2 ha catchment located in the western-central Cascade Mountains of Oregon, at latitude 44°15′N, longitude 122°20′W (Figure 1). WS10 has been the site of intensive research and manipulation by the U.S. Forest Service since the 1960s, mainly designed to study the effects of logging on hydrology, sediment transport, and nutrient loss [*Dyrness*, 1973; *Fredriksen*, 1975; *Harmon et al.*, 1990; *Harr and McCorison*, 1979; *Jones and Grant*, 1996; *Rothacher*, 1965; *Sollins and McCorison*, 1981; *Sollins et al.*, 1981].

[10] Basin elevation ranges from 430 m at the stream gauging station to 700 m at the southeastern ridgeline. Near stream and side slope gradients are approximately 24° and 25° to 50°, respectively [*Grier and Logan*, 1977; *Sollins et al.*, 1981]. The climate is relatively mild with wet winters and dry summers [*Grier and Logan*, 1977]. Mean annual temperature is 8.5°C. Daily temperature extremes vary from 39°C in the summer to −20°C in the winter [*Sollins and McCorison*, 1981]. Mean annual precipitation is 2300 mm and falls primarily as rain between October and April [*Jones and Grant*, 1996]. Total rainfall during June–September averages 200 mm. Snow rarely persists longer than a couple of weeks and usually melts within 1 to 2 days [*Harr and McCorison*, 1979; *Harr et al.*, 1982; *Jones*, 2000]. Average annual streamflow is 1600 mm, which is approximately 70% of annual precipitation.

[11] Soils are of the Frissel series, classified as Typic Dystrochrepts with fine loamy to loamy-skeletal texture [*Sollins et al.*, 1981; *Vanderbilt et al.*, 2003] that are generally deep and well drained [*Grier and Logan*, 1977]. These soils quickly transmit subsurface water to the stream. Subsurface flow is a dominant component of the downslope water movement and is characterized by a strong preferential flow along the soil-bedrock interface [*Van Verseveld et al.*, 2008]. Overland flow rarely occurs [*Harr and McCorison*, 1979].

[12] Prior to the 1975 100% clearcut, WS10 was a 400 to 500 year old forest dominated by Douglas-fir (*Pseudotsuga menziesii*), western hemlock (*Tsuga heterophylla*), and western red cedar (*Thuja plicata*) [*Grier and Logan*, 1977]

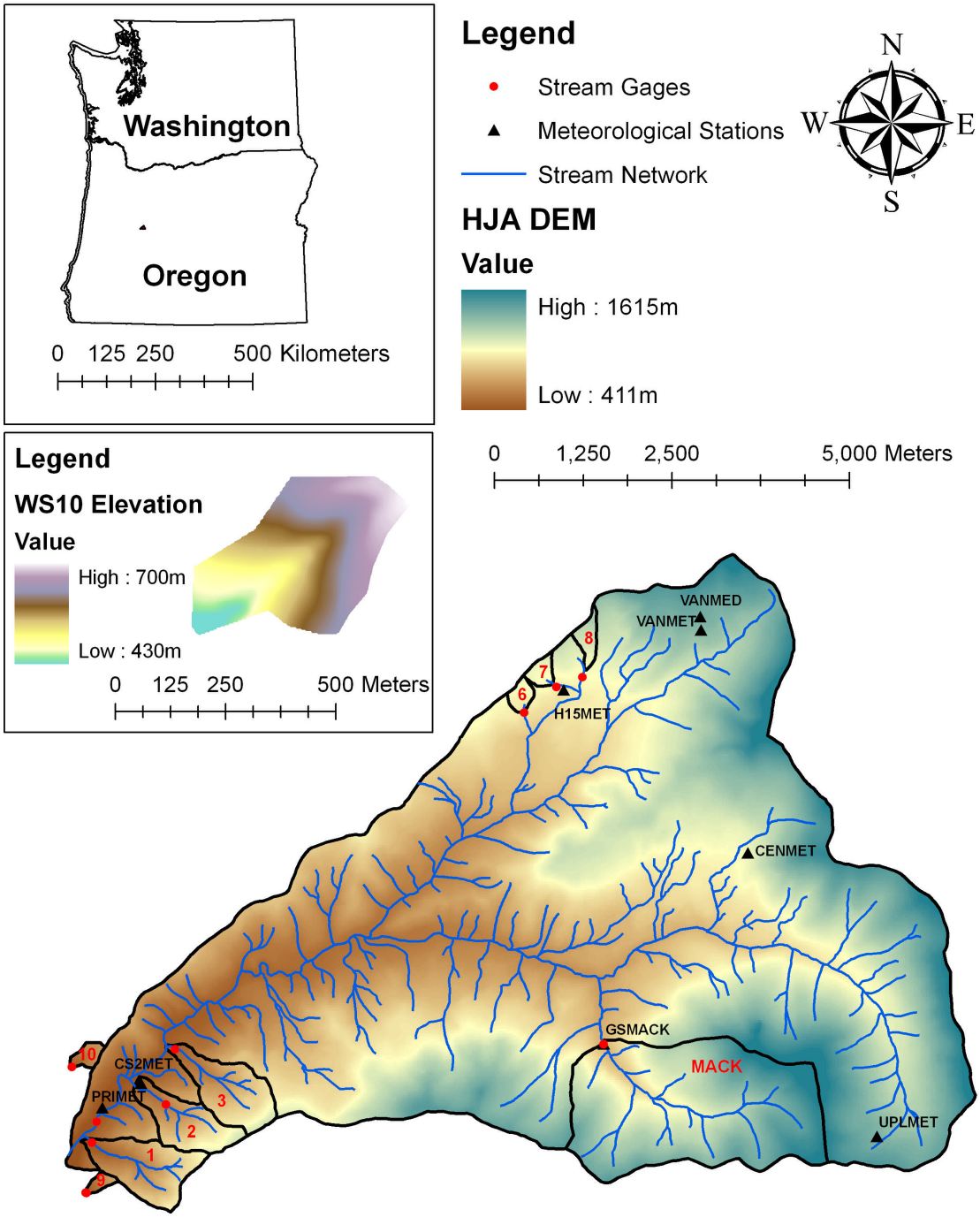

Figure 1. The study site is the watershed 10 (WS10) of the H.J. Andrews Experimental Forest located in the western Cascade Range of Oregon.

reaching up to ~60 m in height. Rooting depths rarely exceed 100 cm [*Santantonio et al.*, 1977]. Species such as the vine maple (*Acer circinatum*), Pacific rhododendron (*Rhododendron maximum*), and chinkapin (*Castanopsis chrysophylla*) regenerated during the spring after logging. Forest regrowth in WS10 was rapid, initially by small trees and shrubs that survived logging, and soon after by planted seedlings of Douglas-fir [*Gholz et al.*, 1985]. The dominant vegetation of WS10 today is a ~35 year old mixed Douglas-fir and western hemlock stand.

3. The Ecohydrological Model

[13] We have developed a spatially distributed ecohydrological model, Visualizing Ecosystems for Land Management Assessment (VELMA), to simulate changes in soil water infiltration and redistribution, evapotranspiration, surface and subsurface runoff, carbon (C) and nitrogen (N) cycling in plants and soils, and the transport of dissolved forms of carbon and nitrogen from the terrestrial landscape to streams. VELMA is designed to simulate the integrated responses of ecohydrologic processes to multiple forcing

variables, e.g., changes in climate, land use, and land cover. It is intended to be broadly applicable to a variety of ecosystems (forest, grassland, agricultural, tundra, etc.) and to provide a computationally efficient means for scaling up ecohydrological responses across multiple spatial and temporal scales—hillslopes to basins, and days to centuries.

[14] VELMA uses a distributed soil column framework to simulate the movement of water and nutrients (NH_4, NO_3, DON, DOC) within the soil, between the soil and the vegetation, and between the soil surface and vegetation to the atmosphere. The soil column model consists of three coupled submodels: (1) a hydrological model that simulates vertical and lateral movement of water within soil, losses of water from soil and vegetation to the atmosphere, and the growth and ablation of the seasonal snowpack, (2) a soil temperature model that simulates daily soil layer temperatures from surface air temperature and snow depth, and (3) a plant-soil model that simulates C and N dynamics. (Note: for the purposes of this paper we describe only the hydrologic aspects of the model.) Each soil column consists of *n* soil layers. Soil water balance is solved for each layer (equations (A1)–(A6)). We employ a simple logistic function that is based on the degree of saturation to capture the breakthrough characteristics of soil water drainage (equations (A7)–(A9)). Evapotranspiration increases exponentially with increasing soil water storage and asymptotically approaches the potential evapotranspiration rate (PET) as water storage reaches saturation [*Davies and Allen*, 1973; *Federer*, 1979, 1982; *Spittlehouse and Black*, 1981] (equation (A12)). PET is estimated using a simple temperature-based method [*Hamon*, 1963] (equation (A13)). An evapotranspiration recovery function is used to account for the effects of changes in stand-level transpiration rates during succession, e.g., after fire or harvest (equation (B2)). Snowmelt is estimated using the degree-day approach [*Rango and Martinec*, 1995] and accounts for the effects of rain on snow [*Harr*, 1981] (equation (A10)).

[15] The soil column model is placed within a catchment framework to create a spatially distributed model applicable to watersheds and landscapes. Adjacent soil columns interact with each other through the downslope lateral transport of water (Figures A1 and A2). Surface and subsurface lateral flow are routed using a multiple flow direction method [*Freeman*, 1991; *Quinn et al.*, 1991]. As with vertical drainage of soil water, lateral subsurface downslope flow is modeled using a simple logistic function multiplied by a factor to account for the local topographic slope angle (equation (A16)). A detailed description of processes and equations is provided in Appendix A.

4. Simulations Methods

4.1. Data

[16] The model is forced with daily temperature and precipitation. Daily observed streamflow data is used to calibrate and validate simulated discharge. For simulations presented here, daily meteorological data for the period 1 January 1969 to 31 December 2008 are obtained from the H.J. Andrews LTER PRIMET, CS2MET, and H15MET meteorological stations located around WS10 [*Daly and McKee*, 2011] (see Figure 1). Daily observed streamflow measurements at WS10 are available from 1969 to 2008 [*Johnson and Rothacher*, 2009]. A 30 m resolution digital elevation model of the H.J. Andrews's watershed 10 [*Valentine and Lienkaemper*, 2005] is used to compute flow direction, delineate watershed boundaries, and generate a channel network. Our soil column is divided into four layers: a surface layer, intermediate layers, and a deep layer. The average soil column depth to bedrock is taken to be 2 m [*Ranken*, 1974]. The dominant soil texture is specified as loam [*Ranken*, 1974]. Porosity, field capacity, and wilting point values are obtained following *Dingman* [1994] (see Table B1).

4.2. Calibration Simulations

[17] Model calibration is needed to accurately capture the pre- and postharvest hydrological dynamics at WS10. This model calibration consists of two simulations: an old-growth simulation for the period 1969–1974 and a postharvest simulation for the period 1975–2008.

[18] The old-growth simulation is conducted for the period 1969 to 1974 in order to calibrate model hydrological parameters such as the surface soil hydraulic conductivity (*Ks*), soil layer thicknesses, ET shape factor, and snowmelt parameters (Table B1). These model parameters are calibrated to (1) reproduce the observed daily streamflow for the period 1969–1974, (2) capture the observed subsurface dynamics in WS10 (i.e., preferential lateral transport of water at the soil-bedrock interface [*Ranken*, 1974; *Van Verseveld et al.*, 2008]), and (3) mimic the rapid runoff response to rainfall [*Kirchner*, 2003; *Ranken*, 1974]. Once this old-growth calibration is complete, model hydrological parameters are considered fixed for the postharvest calibration simulation described below. A detailed description of the catchment hydrological dynamics associated with the old-growth calibration simulation is provided in section 5.1.

[19] The postharvest simulation is conducted for the period 1975 to 2008. This postharvest simulation is used to calibrate those ET recovery function parameters that control postharvest forest regrowth and recovery in transpiration. The ET recovery function parameters are calibrated to reproduce the observed daily streamflow for the period 1975–2008 (see Appendix B for details on the calibration process). Once this final model calibration is complete, all model parameters are considered fixed for all scenarios simulations that explore the impact of harvest amount and location on catchment hydrological processes (see section 5.3). A detailed description of the catchment hydrological dynamic associated with the postharvest calibration simulation is presented in section 5.2. The values of model parameters are provided in Table B1.

5. Simulations Results

5.1. Old-growth Hydrological Dynamics (1969–1974)

[20] Averaged over the period 1969–1974, old-growth evapotranspiration amounts to ~5% (~50 mm) of winter (December–February) precipitation, ~95% (~91 mm) of summer precipitation (June–August), and 35% of annual precipitation. Daily simulated streamflow peaks in November–March due to high precipitation and low evapotranspiration. The largest storm for the 1969–1974 period produces a peak flow of 64 mm day^{-1}. Streamflow rapidly declines in spring–summer as temperatures rise and precipitation

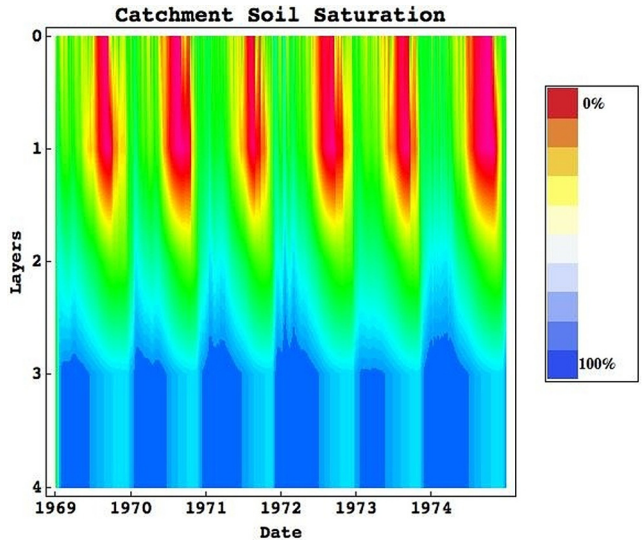

Figure 2. Simulated mean soil water degree of saturation in layer 1, 2, 3, and 4 of the soil column for the old-growth period of 1 January 1969 to 31 December 1974.

diminishes. Summer months are characterized by low flow ($\sim$0.5 mm day^{-1}), high temperatures (reaching 40°C), and low precipitation (less than 8% of annual precipitation). Surface runoff resulting from infiltration excess is rare (<1%). Subsurface flow generated from the surface soil layer, the intermediate soil layers, and the deep soil layer account for $\sim$37%, 32%, and 31% of the annual streamflow, respectively. Soil water content is highest in the winter and lowest in the summer. At the onset of the summer dry period, the surface soil water degree of saturation (SD) declines rapidly from a winter average of 50% to a summer average of 18.5% (Figure 2). Surface SD is the lowest (6%) in August and highest (52%) in December. The SD in the intermediate soil layers is less responsive to changes in precipitation and temperature and exhibits an average time lag of 32 days compared to the surface SD. The SD for these intermediate soil layers is lowest (53%) in September and highest (82%) in February. The SD for the deep soil layer is near saturation (94 $\pm$ 4%) at all times of the year. For this 1969–1974 calibration simulation, the model captures the overall seasonal dynamics of streamflow (Figure 3) with a Nash-Sutcliffe coefficient of 0.807 [*Nash and Sutcliffe*, 1970], a correlation coefficient of 0.907, and an index of agreement of 0.839 [*Willmott*, 1981] (Table 1). The model tends to overpredict low flows and underpredict peak flows.

5.2. Postharvest Hydrological Dynamics (1975–2008)

[21] To examine postharvest hydrological dynamics, two simulations are conducted; a control simulation, for the period 1975 to 2008, in which no vegetation is removed, and a postharvest simulation, also for the period 1975 to 2008, in which vegetation is removed in the spring of 1975. Vegetation removal is simulated by manipulating the ET recovery function to reflect the postclearcut bulk successional dynamics. The function controlling changes in transpiration during forest regrowth is described in Appendix B. Briefly, the transpiration rate is set to zero at the onset of the clearcut and increases asymptotically until reaching predisturbance values at 50 years. Simulation results are presented at daily, monthly, and yearly time scales, in terms of the difference between the postharvest simulation values and the control simulation values. For the postharvest period (1975–2008), the model captures the daily dynamics of streamflow in WS10 (Figure 4) with a Nash-Sutcliffe coefficient of 0.819, a correlation coefficient of 0.913, and an index of agreement of 0.821. Model performance at the daily, monthly, and yearly time scales in simulating postharvest streamflow is presented in Table 1.

[22] On daily time scales, the 1975–1979 fall and winter daily streamflow are on average 1 to 3 mm higher than control values, whereas spring and summer daily streamflow are on average 0.5 to 1.5 mm higher than control values. The maximum daily streamflow surplus of 20 mm (relative to control values) occurs in the fall of 1979. The maximum daily summer streamflow surplus is 2 mm. These initial (1975–1979) summer daily streamflow surpluses switch to deficits after the year 2000, 25 years after clearcut, due to high transpiration rates (higher than old-growth values) associated with young vigorous forest.

[23] On a seasonal basis, absolute changes in streamflow are consistently largest during the fall and winter wet season. For the period 1975–1979, fall and winter streamflow increase by an average of 142 and 90 mm, respectively, whereas summer and spring streamflow increase by an average of 40 and 73 mm, respectively (Figure 5). By contrast,

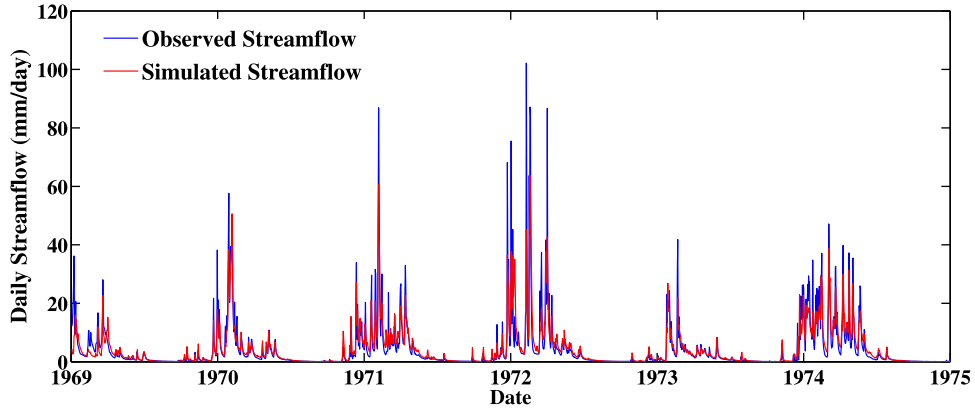

Figure 3. Observed and simulated daily streamflow for the old-growth period of 1 January 1969 to 31 December 1974.

Table 1. Daily, Monthly and Annual Streamflow Modeling Performance for the Old-growth Period (1969–1974) and the Postharvest Period (1975–2008)[a]

Period	Streamflow Modeling Skills for Daily, Monthly and Yearly Time Period				
	Correlation Coefficient R^2	Nash-Sutcliffe Efficiency E_2	First Degree Efficiency E'_1	Baseline Adjusted Index of Agreement d'_1	RMSE
			Old-growth Period (1969–1974)		
Daily flow	0.907	0.807	0.694	0.839	3.854
Monthly flow	0.979	0.955	0.83	0.912	35.04
Annual flow	0.959	0.771	0.444	0.761	120.854
			Postharvest Period (1975–2008)		
Daily flow	0.913	0.819	0.668	0.821	3.341
Monthly flow	0.983	0.963	0.831	0.912	27.163
Annual flow	0.977	0.951	0.786	0.895	87.034

[a]*Nash and Sutcliffe* [1970] defined the coefficient of efficiency E_2, which ranges from minus infinity to 1.0, with higher values indicating better agreement. Values of E_2 are always less than R^2. *Willmott* [1981] developed the index of agreement d'_1, to overcome the insensitivity of correlation-based measures to differences in the observed and simulated means and variances. The index of agreement varies from 0.0 to 1.0, with higher values indicating better agr eement. *Garrick et al.* [1978] defined the baseline adjusted first-degree coefficient of efficiency E'_1, which varies from minus infinity to 1.0, with higher values indicating better agreement. A detailed description of these coefficients can be found in the papers by *Legates and McCabe Jr.* [1999] and *Waichler et al.* [2005].

relative changes in streamflow are largest in the summer averaging 140% for the first five years after harvest and smallest in the winter at approximately 15% (Figure 6). Relative increases in fall and spring streamflow are intermediate at 36% and 40%, respectively, for the first five years after harvest (Figure 6). By the year 2000, 25 years after harvest, simulated changes in summer and fall streamflow are negative (i.e., lower than control values) as a result of increasing rates of transpiration during forest regrowth (Figure 5). As the forest matures, simulated transpiration rates approach old-growth levels, such that changes in summer streamflow are similar to control values.

[24] For the first five years after disturbance, average seasonal changes in SD are largest in the summer and fall, with average increases of 18% and 14%, respectively. Winter and spring SD increase by an average of only 5%. Twenty-five years after clearcut, summer and fall SD changes are negative (i.e., less than control values). Negative relative changes in SD develop in June and are most intense (∼−1.5%) in July, August, September, and October. By the end of October, negative relative changes in SD are less than 0.6% but last until the end of November.

[25] On an annual scale, simulated annual average evapotranspiration decreases by ∼43% or 370 mm year^{-1} for the period 1975–1979. Consequently, average annual streamflow increases by ∼29% or 345 mm year^{-1} during the same period. In the first year after disturbance, annual streamflow increases by 326 mm. Average increase in annual streamflow peaks two years after clearcut and reaches ∼500 mm as a result of high precipitation and low evapotranspiration demands. Thereafter, changes in annual streamflow decline. Thirty years after disturbance, simulated postharvest streamflow is approximately equal to simulated control streamflow (Figures 5 and 6). Simulated deep subsurface flow (i.e., flow at the soil-bedrock interface) is the major contributor to the postharvest increase in streamflow. Simulated deep subsurface flow increases by an average of 50% after clearcut. By contrast, changes in subsurface flow for surface and intermediate layers are less than 20%. Thirty years after harvest, changes in subsurface flow are within 1% of control values. Simulated annual catchment SD increases by an average of 12% for the period 1975–1979. The largest increase in soil water degree of saturation is in the intermediate layers, with an annual average increase of 15%. By contrast,

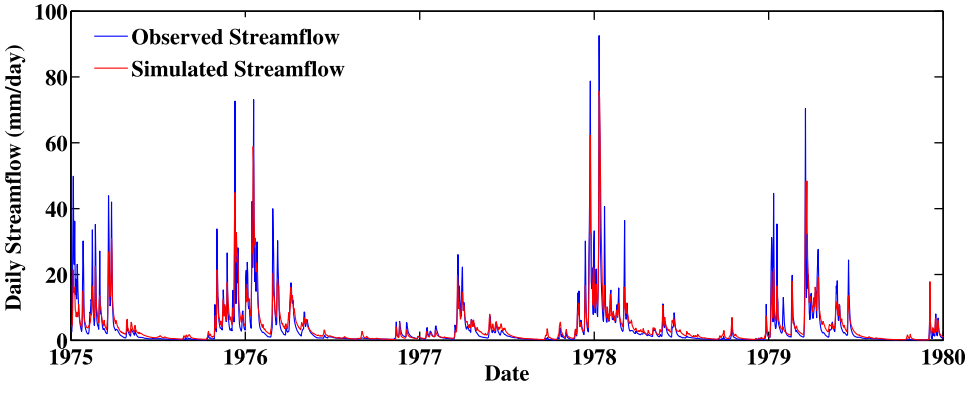

Figure 4. Observed and simulated daily streamflow for the postclearcut period of 1 January 1975 to 31 December 1979. For the postharvest period (1975–2008), the model captures the daily streamflow dynamics with a Nash-Sutcliffe coefficient of 0.82, a correlation coefficient of 0.91, and an index of agreement of 0.82.

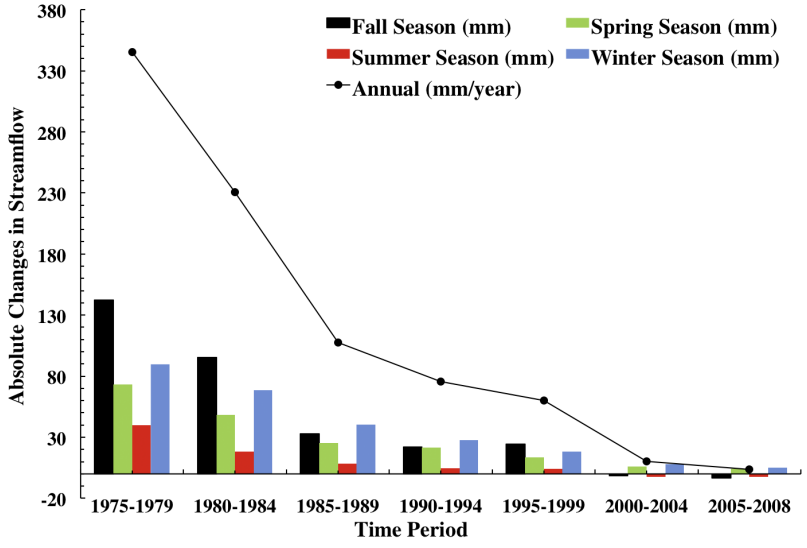

Figure 5. Simulated seasonal and annual absolute changes in streamflow for the old-growth period of 1975 to 2008.

simulated SD in the soil surface and deep layers increases by 7% and 5%, respectively.

5.3. Harvest Scenarios Simulations

[26] The harvest location and amount simulations described below are forced with WS10 precipitation and air temperature data for the period 1975–2008.

5.3.1. Harvest Location

[27] To assess the impact of harvest location on stream discharge, 20 simulations scenarios are conducted. Each scenario has the harvest amount fixed at 20% of the catchment area. However, harvest location within the watershed varies. The location of each 20% clearcut varies from an all ridge location (Figure 7; scenario A) to an all valley location (Figure 7; scenario T). Catchment pixels within a 20% clearcut are based on flow accumulation.

[28] Simulation results show that forest harvest location is important. A 20% clearcut in the uplands (an average distance of 152 m to the nearest stream channel, based on flow direction) results in an average annual streamflow increase of ~54 mm or 4% over the first five years after clearcut (1975–1979). By contrast, a 20% clearcut in the lowlands (an average distance of 53 m from the nearest stream channel, based on flow direction) results in an average annual streamflow increase of ~92 mm or 8% over the same period. Taken together, these 20 simulations suggest a linear increase in streamflow as the clearcut location shifts from the uplands to the lowlands (Figure 8; correlation coefficient $R^2 = 0.97$).

5.3.2. Harvest Amount

[29] To assess the impact of harvest amount on stream discharge, evapotranspiration and SD, 100 virtual harvest

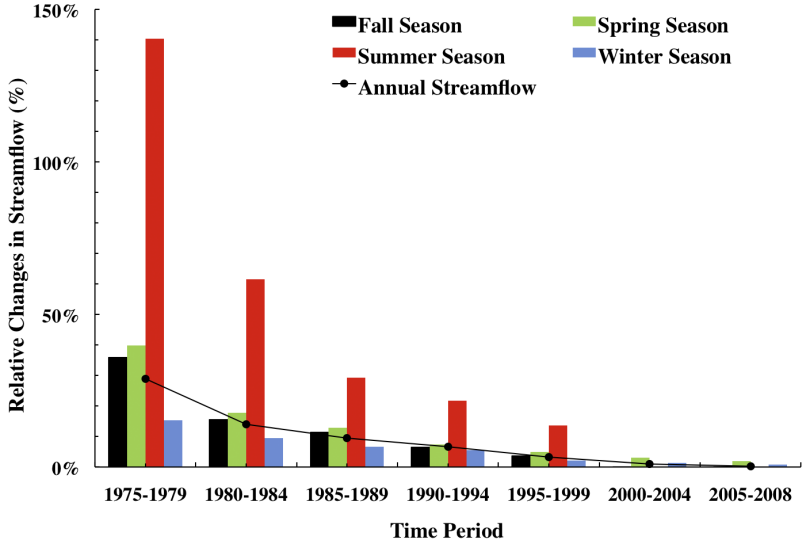

Figure 6. Simulated seasonal and annual relative changes in streamflow for the postclearcut period of 1975 to 2008.

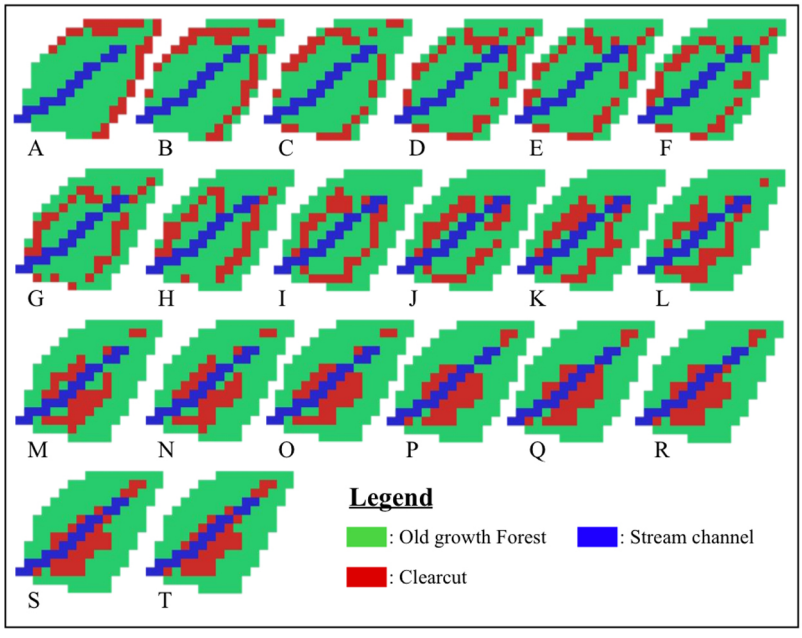

Figure 7. Spatial pattern of forest harvest. Twenty scenarios of 20% clearcut area each were simulated. The location of the 20% clearcut area varied from an all ridge location (scenario A) to an all valley location (scenario T).

amount scenarios are simulated. Fifty harvest amount scenarios ranging from 2% to 100%, with an approximate increment of 2% in harvest area, are simulated from ridge to valley (Figure 9). Thereafter, 50 harvest amount scenarios ranging from 2% to 100%, with an approximate increment of 2% in harvest area, are simulated from valley to ridge (Figure 9). Catchment pixels for a given clearcut amount are based on flow accumulation.

[30] For ridge-to-valley simulations, the relationship between the change in annual streamflow and harvest area is near linear (correlation coefficient $R^2 = 0.97$), with a slight convex curvature (Figure 10). Specifically, average annual streamflow increases by ~2 mm for each 1% of catchment area harvested near the ridge, but by ~4 mm for each 1% of catchment area harvested near the valley. The negative relationship between annual evapotranspiration and harvest area is also near linear (correlation coefficient $R^2 = 0.98$), with a slight concave curvature (Figure 10). In particular, average annual evapotranspiration decreases by ~3 mm for each 1% of catchment area harvested near the ridge, but by ~4 mm for each 1% of catchment area harvested near the valley.

[31] For valley-to-ridge simulations, the relationship between the change in annual streamflow and harvest area is near linear (correlation coefficient $R^2 = 0.98$), with a slight concave curvature (Figure 10). Specifically, average annual streamflow increases by ~4 mm for each 1% of catchment area harvested near the valley, but by ~3 mm for each 1% of catchment area harvested near the ridge. The negative relationship between annual evapotranspiration and harvest area is also near linear (correlation coefficient $R^2 = 0.98$), with a slight convex curvature (Figure 10). In particular, average annual evapotranspiration decreases by ~5 mm for each 1% of catchment area harvested near the valley, but by ~3 mm for each 1% of catchment area harvested near the ridge.

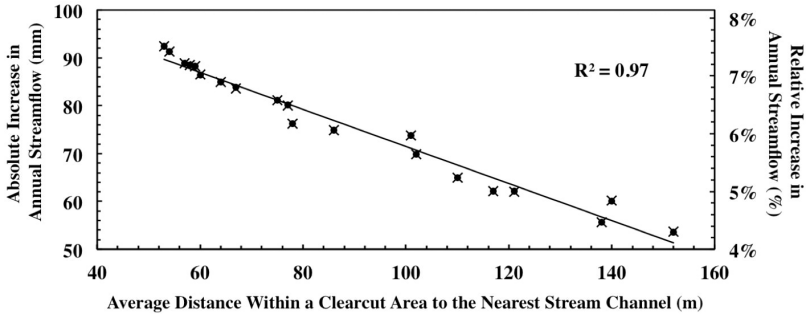

Figure 8. Absolute and relative increase in annual streamflow for a 20% clearcut as a function of the average flow path distance in meters between the harvest area and the nearest stream channel. The solid black line is the fitted linear trendline.

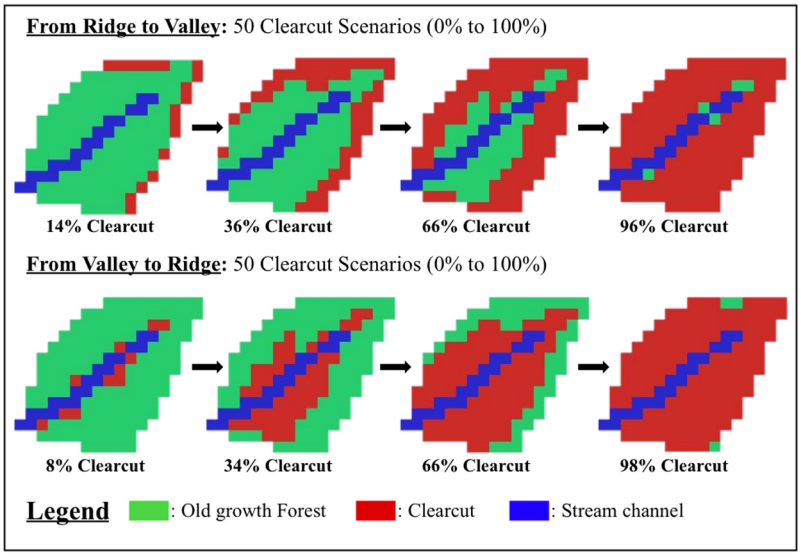

Figure 9. Harvest amount scenarios. Selected examples of 50 clearcut scenarios ranging from 0% to 100% with a ~2% increment in harvest area were simulated (1) from ridge to valley, and (2) from valley to ridge, to assess the impact of increasing harvest area on catchment hydrological response.

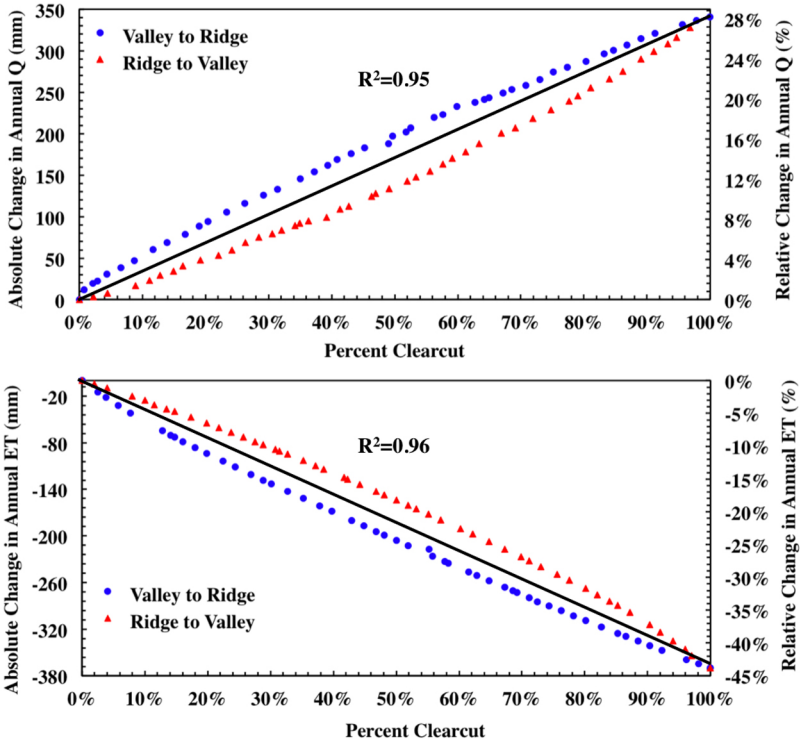

Figure 10. Simulated absolute and relative increase in average annual streamflow (Q), and average annual evapotranspiration (ET) as a function of harvest area, over the first five years after clearcut. The red triangles represent the ridge-to-valley simulations results. The blue dots represent the valley-to-ridge simulations results. The solid black line is the fitted linear trendline.

[32] While there are some differences between the ridge-to-valley and the valley-to-ridge simulations (Figure 10), together they suggest that, irrespective of location: (1) annual streamflow increases linearly at a rate of ~3.5 mm year^{-1} for each percentage of catchment harvested, (2) annual evapotranspiration decreases linearly at a rate of ~3.6 mm year^{-1} for each 1% of catchment area harvested, and (3) whole catchment SD increases linearly at a rate of 1.2% for each 1% of catchment area harvested (not shown). Moreover, there are no apparent hydrologic thresholds that lead to a nonlinear streamflow response to increasing harvest amount.

[33] Considering all harvest amount scenarios, the absolute changes in streamflow are largest during the fall-winter wet season, whereas the largest relative changes in streamflow are in summer months just after clearcut (Figure 11). In the first five years after clearcut, maximum daily increases in streamflow range from 1 to 20 mm for a 2% and 100% harvest scenario, respectively. Changes in SD are most pronounced in the intermediate layers of the soil column and during the summer and fall seasons. Thirty years after disturbance, simulated postharvest streamflow, evapotranspiration, and SD are near simulated control values.

6. Discussion

[34] We use a spatially distributed ecohydrologic model, VELMA, to analyze the effects of harvest amount and location on catchment hydrological processes at an intensively studied 10 ha catchment in the western Oregon Cascades that was clearcut in 1975. Comparison of 40 years of modeled and observed streamflow data show that VELMA captures daily, seasonal, and annual streamflow dynamics for both the pre- (1969–1974) and postharvest (1975–2008) periods. Multiple simulation scenarios are conducted to explore the effects of harvest amount and location on catchment hydrological response. Results show that: (1) for

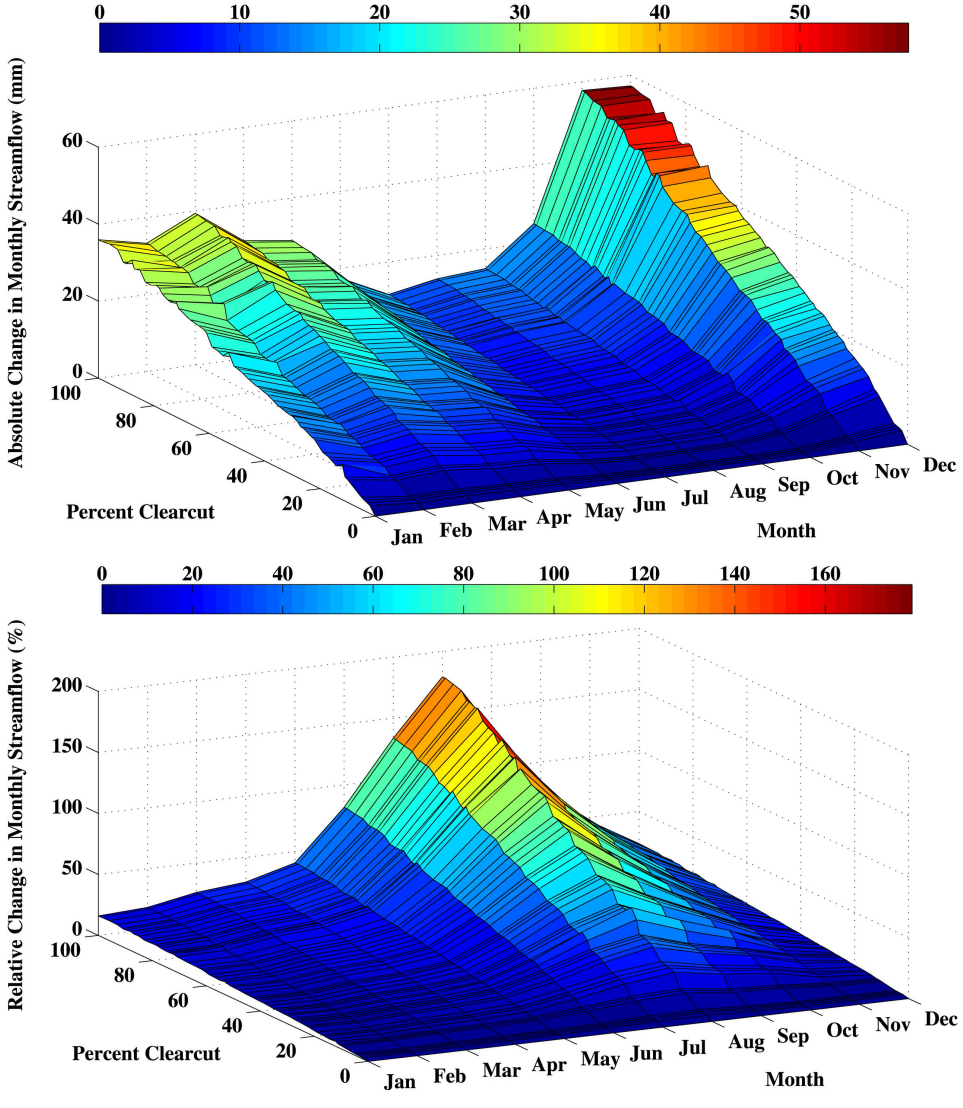

Figure 11. Simulated absolute and relative increase in monthly streamflow as a function of harvest area, in the 1–5 years after clearcut (1975–1979).

the case of a 100% clearcut, stream discharge initially increases by ~29% or 345 mm but returns to old-growth levels within 50 years (Figures 5 and 6), (2) fall increases in streamflow are large in absolute terms, whereas summer increases are large in relative terms (Figure 11), (3) annual streamflow increases linearly at a rate of 3.5 mm year^{-1} for each percent of catchment harvested, irrespective of location (Figure 10), (4) the increase in annual streamflow is small (less than 40 mm year^{-1}) for harvest amounts of less than 10% (Figure 10), and (5) streamflow response is strongly sensitive to harvest distance from the stream channel (Figure 8).

[35] For our WS10 simulations, results suggest that streamflow increases linearly with harvest amount, irrespective of location, and is insignificant for a harvest area of less than 10% (Figure 10). *Stednick* [1996], who reviewed 95 paired-catchment studies across the United States, also found that annual streamflow increased linearly with increasing harvest area, and that changes in annual streamflow in the Pacific Northwest catchments were undetectable for harvest areas of less than 20%. *Bosch and Hewlett* [1982] reviewed 94 paired-catchment studies in Asia, Australia, Africa, and North America, and found that annual water yield increased by ~40 mm for every 10% reduction in coniferous forest cover. Likewise, *Sahin and Hall* [1996] analyzed the results of 145 experimental studies in Asia, Australia, Africa, Europe, and North America, and found that annual streamflow increased linearly at a rate of 20 to 25 mm year^{-1} for each 10% reduction in coniferous forest cover. *Grant et al.* [2008] analyzed the results of several experimental and modeling studies across the Pacific Northwest and found that the change in peak flow increased linearly with increasing harvest area and was undetectable (i.e., relative change in peakflow is less than 10%) for harvested areas of less than 29% in rain dominated catchments and 15% for catchments in the transient snow zone.

[36] For our WS10 simulations, the largest absolute increase in streamflow is in fall and winter, while the largest relative increase in streamflow is associated with summer months. Similar results have been found by *Harr et al.* [1979], who examined the seasonal changes in streamflow following a 100% clearcut of two Coyote Creek experimental watersheds in Southwest Oregon. *Harr et al.* [1979] found that the largest absolute increase in streamflow (~120 mm) was in winter, whereas the largest relative increase (~44%) was in the low flow summer months. Likewise, *Jones and Post* [2004] examined the seasonality of streamflow to forest clearcut in 14 experimental paired watersheds located in northwest conifer and eastern deciduous forests. They found that the absolute increase in streamflow was largest in moist seasons, whereas the relative increase in streamflow was highest in the warm seasons.

[37] Our simulation results suggest that postclearcut annual streamflow increases with decreasing harvest distance to the channel (Figure 8). This streamflow sensitivity to harvest location stems from the fact that subsurface flow generated from an upland clearcut area, as opposed to a lowland clearcut area, has a relatively longer flow path. This longer flow path subjects subsurface flow to downslope plant water uptake, which reduces the amount of water that reaches the stream channel. These results are consistent with previous findings on the importance of riparian forest buffers and lowland vegetation in reducing subsurface flow to streams [*Jordan et al.*, 1993; *Lowrance et al.*, 1997].

[38] Forest harvest effects on streamflow in WS10 were simulated in a simplified way, with the ultimate goal of developing a framework that can be efficiently scaled up for larger watersheds of interest to land managers and policy makers. For example, one of our objectives is to provide a foundation for extrapolation to managed landscapes that are not as data rich as LTER sites (e.g., ungauged basins with little soil and vegetation data). However, our simplifying assumptions need to be examined. Below we discuss a number of harvest effects and watershed characteristics relevant to hydrological processes not explicitly addressed in this study.

[39] 1. Roads. The impact of forest roads on hydrological processes have been well documented for the H.J. Andrews Experimental Forest [*Jones and Grant*, 1996; *Luce and Wemple*, 2001; *Swanson and Dyrness*, 1975; *Wemple and Jones*, 2003; *Wemple et al.*, 2001]. Roads have been shown to (1) intercept and route surface and shallow subsurface water to stream channels [*Luce and Wemple*, 2001], (2) increase the magnitude and frequency of peak flows [*Jones and Grant*, 1996], and (3) increase sediment transport to the stream [*Beschta*, 1978; *Swanston and Swanson*, 1976].

[40] 2. Harvest methods. Forest harvest in many Pacific Northwest sites is conducted with skidders, tractors, or cable yarding [*Moore and Wondzell*, 2005]. WS10 was logged using a skyline cable system [*Hood et al.*, 2006], and trees were felled and dragged uphill to a single landing [*Sollins and McCorison*, 1981]. As a result, soils on about 50% of the watershed were subjected to moderate or severe disturbance or compaction [*Harr and McCorison*, 1979]. Such soil compaction reduces soil infiltration capacity [*Startsev and McNabb*, 2000], saturated hydraulic conductivity [*Purser and Cundy*, 1992], pore size distribution, and pore space [*Huang et al.*, 1996], which in turn, impact watershed hydrological processes.

[41] 3. Forest succession. Biomass recovery is complex, involving changes in species composition, growth rates, and canopy structure. During postclearcut succession, species composition often changes from colonizing shrubs to hardwood trees before returning to conifer dominance [*Yang et al.*, 2005]. To accurately model these successional dynamics would require the inclusion of multiple species, species interaction, overstory and understory dynamics, the seasonality of leaf area, and canopy interception, among others [*Bond-Lamberty et al.*, 2005]. However, including these dynamics would increase model complexity, decrease computational efficiency, and limit model application to sites rich in data. Instead our simulations use a Chapman-Richards growth function [*Hunt*, 1982; *Ratkowsky*, 1990; *Richards*, 1959] that relates canopy transpiration to forest age, as a simple proxy for plant/biomass recovery (equation (B2)).

[42] 4. Soil spatial heterogeneity. Soil texture and depth vary spatially within WS10 [*McGuire et al.*, 2007; *Ranken*, 1974; *Sayama and McDonnell*, 2009]. However, deriving high-resolution and catchment wide soil texture and depth maps from, typically, a small number of point measurements, is at best, uncertain. Instead, we assume uniform loam soil texture and uniform depth to bedrock of 2 m to reflect, more or less, average conditions in the catchment [*Ranken*, 1974]. While a sensitivity analysis on the impact

of the spatial distribution of soil texture and soil depth on streamflow dynamics would certainly provide insights into catchment dynamics, it is beyond the scope of this paper.

[43] Finally, it is important to ask whether or not an explicit treatment of the preceding issues would improve model performance and the understanding of process-level controls on streamflow and other ecohydrological processes. For some applications, the explicit treatment of these processes may be needed. However, it must be recognized that such added processes come at the cost of computational efficiency, model complexity, and applicability to larger spatial and temporal scales. The current version of VELMA is an initial attempt at a parsimonious solution to this dilemma.

7. Conclusion

[44] Despite the limitations discussed above, the model presented here provides a relatively simple, spatially distributed framework for assessing the effects of changes in climate, land use, and land cover on ecohydrological processes within watersheds. The WS10 simulations suggest that the model can predict, with reasonable accuracy, the effects of forest harvest on daily, seasonal, and annual changes in streamflow. The simulations describing the effects of harvest amount and spatial pattern provide process-level insights into important hydrological responses to harvest—details that would be difficult or impossible to capture through experimentation or observation alone. Moreover, the model provides an integrated ecohydrological framework for evaluating how alternative climate and forest management scenarios may interact to affect the functioning and health of forest and stream ecosystems. Finally, the simplicity of the model makes it potentially useful for applications across a range of spatial and temporal scales relevant to land managers and policy makers.

Appendix A: Model Description

[45] We include two appendices. Appendix A describes the hydrology model, which includes the equations typically applied across watersheds and ecosystems. Appendix B describes the evapotranspiration recovery function used to mimic postharvest transpiration dynamics.

[46] VELMA is a spatially distributed ecohydrology model that accounts for hydrologic and biogeochemical processes within watersheds. The model simulates daily to century-scale changes in soil water storage, surface and subsurface runoff, vertical drainage, carbon (C) and nitrogen (N) cycling in plants and soils, as well as transport of nutrients from the terrestrial landscape to the streams. VELMA consists of multilayered soil column models that communicate with each other through the downslope lateral transport of water (Figure A1). Each soil column model consists of three coupled submodels: a hydrological model, a soil temperature model, and a plant-soil model. What we describe below is the hydrology component of the model. First, we describe the soil column model and then place this soil column within a catchment framework.

A1. The Hydrological Model

A1.1. Soil Column Framework

[47] We employ a multilayer soil column as the fundamental hydrologic unit. The soil column consists of n soil layers, a standing water layer, and a snow layer (Figure A2). Soil water balance is solved for each model layer (equations (A1)–(A6)). Soil water storage in layer i (s_i), surface standing water (s_{STW}), and snow water equivalent (s_{SWE}), are tracked and updated at each time step. For a four-layer soil model, such as the one used in this work:

$$\frac{ds_{\mathrm{SWE}}}{dt} = P_s - m, \tag{A1}$$

$$\frac{ds_{\mathrm{STW}}}{dt} = P_r - I + m - Q_{s\_\mathrm{out}} + Q_{s\_\mathrm{in}}, \tag{A2}$$

$$\frac{ds_1}{dt} = I - D_1 - ET_1 - Q_{1\_\mathrm{out}} + Q_{1\_\mathrm{in}}, \tag{A3}$$

$$\frac{ds_2}{dt} = D_1 - D_2 - ET_2 - Q_{2\_\mathrm{out}} + Q_{2\_\mathrm{in}}, \tag{A4}$$

$$\frac{ds_3}{dt} = D_2 - D_3 - ET_3 - Q_{3\_\mathrm{out}} + Q_{3\_\mathrm{in}}, \tag{A5}$$

$$\frac{ds_4}{dt} = D_3 - Q_{4\_\mathrm{out}} + Q_{4\_\mathrm{in}}, \tag{A6}$$

where P_r (mm day^{-1}) and P_s (mm day^{-1}) are rain and snow, respectively, ET_i (mm day^{-1}) is the water extracted from soil layer i due to evapotranspiration, s_i (mm) is the soil water storage in layer i; s_{SWE} (mm) is the snow water equivalent due to the accumulation of snow, s_{STW} (mm) is

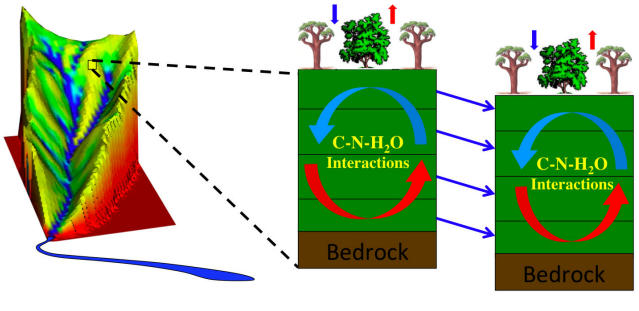

Figure A1. Conceptual catchment modeling framework using multilayered soil columns.

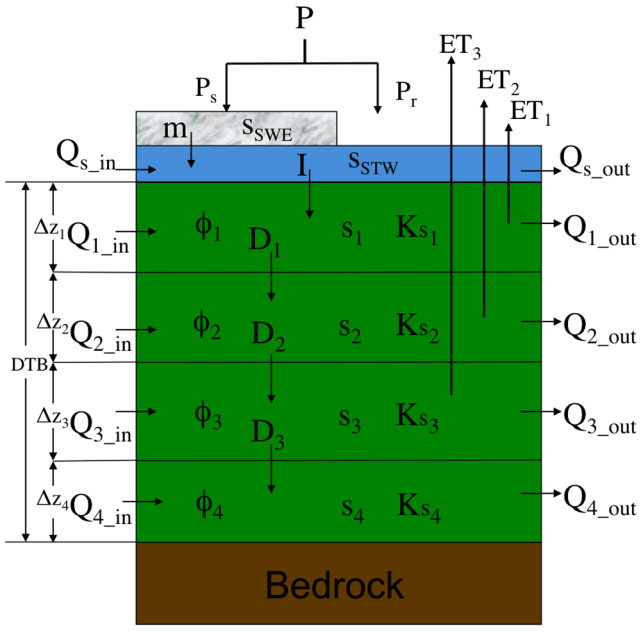

Figure A2. The soil column framework consists of four-layer soil column, a standing water layer, and a snow layer. DTB is the soil column depth to bedrock. z_i, Ks_i, ϕ_i, and s_i are the thickness, the saturated hydraulic conductivity, the soil porosity, and the soil water storage of layer i, respectively.

the standing water amount, m (mm day^{-1}) is the snowmelt that enters the standing water layer, I (mm day^{-1}) is the soil infiltration rate, D_i (mm day^{-1}) is the vertical drainage from layer i to layer $i+1$ within a given soil column, Q_{i_in} (mm day^{-1}) and Q_{i_out} (mm day^{-1}) are the lateral subsurface flow into and out of layer i; Q_{s_in} (mm day^{-1}) is the surface water flow from the s_{STW} pool of an upslope soil column, and Q_{s_out} (mm day^{-1}) is the surface water flow to the s_{STW} pool of a downslope soil column or into the stream.

A1.2. Vertical Water Drainage

[48] The vertical water drainage (D_i) is modeled using a logistic function that is intended to capture the breakthrough characteristics of soil water movement. Specifically, we employ a logistic function $f\left(s_i/s_i^{\max}\right)$ that permits for fast "switching" from low to high flow as layer water storage approaches field capacity:

$$D_i = Ks_i^{\text{vertical}} \times f\left(s_i/s_i^{\max}\right) \qquad i = 1, 2, \ldots, n, \tag{A7}$$

where Ks_i^{vertical} is the vertical saturated hydraulic conductivity in layer i, $\left(s_i/s_i^{\max}\right)$ is the soil degree of saturation in layer i, $s_i^{\max}$ (mm) is the maximum soil water storage in layer i, and $f\left(s_i/s_i^{\max}\right)$ is the logistic function for layer i. The vertical saturated hydraulic conductivity follows a TOPMODEL framework [*Beven and Kirkby*, 1979] and decreases exponentially with depth such that

$$Ks_i^{\text{vertical}} = Ks \times e^{-f_v \times d_i} \qquad i = 1, 2, \ldots, n, \tag{A8}$$

where Ks is the soil surface saturated hydraulic conductivity [*Clapp and Hornberger*, 1978; *Dingman*, 1994], f_v is the vertical decay rate of Ks with depth, and d_i is the soil depth to the center of layer i.

[49] The logistic function is modeled as

$$f\left(s_i/s_i^{\max}\right) = \frac{1+\exp\left[-\left(s_i/s_i^{\max}\right)\right]}{1+a_{1,i}\exp\left[-a_{2,i}\left(s_i/s_i^{\max}\right)\right]} - \frac{2}{\left(1+a_{1,i}\right)} \quad i = 1, 2, \ldots, n$$
$$\text{with} \begin{cases} a_{1,i} = \exp\left[6 + 270.562 \times \left(Ks_i^{\text{vertical}}\right)^{-0.574}\right] \\ a_{2,i} = 6 + 144.749 \times \left(Ks_i^{\text{vertical}}\right)^{-0.444}. \end{cases} \tag{A9}$$

A1.3. Precipitation, Rain, Snow, and Snowmelt

[50] Below a threshold temperature (T_{th}), precipitation (P) falls as snow (P_s), otherwise as rain (P_r). Snow accumulates until air temperature (T_a) warms and reaches melting temperature (T_m). Snowmelt rate (m) follows a degree day approach [*Rango and Martinec*, 1995], and includes for the heat provided by rain on snow [*Harr*, 1981]. Snowmelt (m) enters the s_{STW} pool and from there infiltrates into the top soil layer (or continues as lateral surface flow and enters a downslope s_{STW} pool, section 2.2)

$$P = \begin{cases} P_r & T_a > T_{\text{th}} \\ P_s & T_a \le T_{\text{th}} \end{cases}$$
$$m = \begin{cases} \alpha(T_a - T_m) + \sigma \times P_r \times T_a & T_a > T_m \\ 0 & T_a \le T_m, \end{cases} \tag{A10}$$

where α (mm°C^{-1} day^{-1}) is the degree-day factor for melt and σ is the rain on snow factor.

A1.4. Surface Soil Infiltration

[51] Based on the large uncertainties associated in ascribing soil texture, soil structure, and soil properties, we simply

assume that water stored in the s_{STW} pool is allowed to infiltrate (I) the top soil layer such that:

$$\begin{aligned} I &= (P_r + m + Q_{s\_\mathrm{in}} - Q_{s\_\mathrm{out}}) \\ &\quad \text{for } (P_r + m + Q_{s\_\mathrm{in}} - Q_{s\_\mathrm{out}}) < Ks_{i=1}^{\mathrm{vertical}} \\ I &= Ks_{i=1}^{\mathrm{vertical}} \\ &\quad \text{for } (P_r + m + Q_{s\_\mathrm{in}} - Q_{s\_\mathrm{out}}) \geq Ks_{i=1}^{\mathrm{vertical}}. \end{aligned} \tag{A11}$$

A1.5. Evapotranspiration

[52] Evapotranspiration increases exponentially with increasing soil water storage and asymptotically approaches the potential evapotranspiration (PET) rate as water storage reaches saturation [*Davies and Allen*, 1973; *Federer*, 1979, 1982; *Spittlehouse and Black*, 1981]:

$$\begin{aligned} ET_i &= W_{E,i} \times PET \times \left\{1 - \exp\left[-c_{ET} \times \left(s_i / s_i^{\max}\right)\right]\right\} \\ &\quad i = 1, 2, \ldots, n, \end{aligned} \tag{A12}$$

where $W_{E,i}$ is the soil water extraction fraction in layer i and c_{ET} is an ET shape factor to ensure that ET approaches PET near field capacity.

[53] PET is estimated using a simple temperature-based method [*Hamon*, 1963]:

$$\begin{aligned} PET &= K_{PET} \times 0.0138 \times L \times \rho_{\mathrm{vsat}}(T_a) \\ \text{with} &\quad \begin{cases} \rho_{\mathrm{vsat}}(T_a) = 0.622 \times \rho_a \times \left(\dfrac{e_{\mathrm{sat}}(T_a)}{p_{\mathrm{SL}}}\right) \\ e_{\mathrm{sat}}(T_a) = 6.11 \times \exp\left(\dfrac{17.3 \times T_a}{T_a + 273.3}\right) \end{cases}, \end{aligned} \tag{A13}$$

where $\rho_{\mathrm{vsat}}(T_a)$ is the saturation absolute humidity (g m^{-3}) at the mean daily air temperature T_a (°C), ρ_a is the air density (1300 g m^{-3}), $e_{\mathrm{sat}}(T_a)$ is the saturation vapor pressure (kPa) at T_a, p_{SL} is the mean pressure at sea level (101.3 kPa), K_{PET} is a calibration constant, and L is the local day length expressed in hours [*Dingman*, 1994].

[54] The distribution of plant water extraction through the soil profile has a significant impact on the ability of vegetation to access water throughout the growing season [*Bond et al.*, 2008]. Roots, soil macropores, and soil saturated hydraulic conductivity all tend to fall off exponentially with depth [*Beven and Kirkby*, 1979; *Gale and Grigal*, 1987; *Jackson et al.*, 1996; *Sidle et al.*, 2001; *Wigmosta and Perkins*, 2001], which suggests that the ability to extract water from the soil column decreases with soil depth. A number of studies have found that the majority of water uptake is in the shallow soils where water and nutrients are abundant [*Jackson et al.*, 1996; *Warren et al.*, 2005]. However, these studies also suggest that water uptake shifts from shallow to deep layers as near surface soils dry out [*Brooks et al.*, 2006; *Hacke et al.*, 2000; *Warren et al.*, 2005]. To mimic these dynamics, soil water uptake is modeled as follows:

$$\begin{aligned} &\text{for } \left(\frac{s_{i=(d_r-1)}}{s_{i=(d_r-1)}^{\max}}\right) \geq \left(\frac{\theta_{i=(d_r-1)}^{w}}{\varphi_{i=(d_r-1)}}\right) \\ &\quad \begin{cases} W_{E,i} = \dfrac{s_i}{\sum_{j=1}^{d_r-1} s_j} & i = 1, 2, \ldots, (d_r - 1) \\ W_{E,i} = 0 & i = d_r, \ldots, n, \end{cases} \end{aligned} \tag{A14}$$

$$\begin{aligned} &\text{for } \left(\frac{s_{i=(d_r-1)}}{s_{i=(d_r-1)}^{\max}}\right) < \left(\frac{\theta_{i=(d_r-1)}^{w}}{\varphi_{i=(d_r-1)}}\right) \\ &\quad \begin{cases} W_{E,i} = \dfrac{\left(1 - W_{E,\mathrm{deep}}\right) \times s_i}{\sum_{j=1}^{d_r-1} s_j} & i = 1, 2, \ldots, (d_r - 1) \\ W_{E,i} = W_{E,\mathrm{deep}} & i = d_r \\ W_{E,i} = 0 & i = (d_r + 1), \ldots, n, \end{cases} \end{aligned} \tag{A15}$$

where θ_i^w and φ_i are the soil wilting point and the soil porosity in layer i, respectively, layer d_r is the deepest layer in which water extraction is possible, $\left(s_{i=(d_r-1)} \Big/ s_{i=(d_r-1)}^{\max}\right)$ is the degree of saturation of layer $(d_r - 1)$, and $W_{E,\mathrm{deep}}$ is the fraction of water uptake from layer d_r during droughts (a calibrated value). The depth of layer d_r is determined either experimentally (typically taken from rooting depth information) or through calibration. Based on equation (A14), water uptake is limited to shallow layers as long as water storage in these layers is above wilting point. When the water storage in the shallow layers is below wilting point, equation (A15) permits for deep soil water extraction.

A2. Watershed Framework

[55] To place the above described soil column framework within a catchment framework, the catchment topography is gridded into a number of pixels (dependent upon the available DEM, e.g., 30 m), with each pixel consisting of one soil column model (Figure A1). Soil columns communicate with each other through the downslope lateral transport of water. For simplicity, lateral subsurface flow Q_i (equation (A16)) from one soil column pixel to a downslope neighbor is from layer i of the upslope pixel to layer i of the downslope pixel. Lateral surface flow Q_s (equation (A18)) is from the s_{STW} pool of an upslope pixel to the s_{STW} pool of a downslope pixel, where it can then either infiltrate into the top soil layer of the downslope pixel, or continue its downslope movement as lateral surface flow. A multiple flow direction method is used where flow from one pixel to its eight neighbors is fractionally allocated according to terrain slope [*Freeman*, 1991; *Quinn et al.*, 1991].

A2.1. Lateral Subsurface Runoff

[56] Lateral downslope flow (Q_i) is triggered near field capacity using the logistic function presented in equation (A9) but (1) corrected for the local slope and (2) Ks_i^{vertical} in $a_{1,I}$ and $a_{2,i}$ is replaced by Ks_i^{lateral} such that

$$Q_i = Ks_i^{\mathrm{lateral}} \times SL \times f\left(s_i / s_i^{\max}\right) \qquad i = 1, 2, \ldots, n \tag{A16}$$

and

$$Ks_i^{\mathrm{lateral}} = Ks \times e^{-f_l \times d_i} \qquad i = 1, 2, \ldots, n, \tag{A17}$$

where Ks_i^{lateral} is the lateral saturated hydraulic conductivity in layer i, SL is the local terrain slope, and f_l is the lateral decay rate of Ks with depth.

A2.2. Surface Runoff

[57] Surface runoff (Q_s) from a pixel is a product of the standing water after infiltration (I) is accounted for, the local terrain slope, and the Chezy "like" coefficient (Che) (1/time) [*Dingman*, 1994]:

$$Q_s = Che \times SL \times s_{\mathrm{STW}}. \tag{A18}$$

A2.3. Total Runoff

[58] Total catchment discharge (Q_T) is computed as the sum of the lateral flows into the channel, the rain falling directly on the channel, and the snowmelt from channel pixels. The stream channel is defined as all pixels with a flow accumulation area above a predefined threshold. We assume that all flows entering the channel are directly routed to the outlet such that

$$Q_T = \sum_{j=1}^{cn} \sum_{i=1}^{n} (Q_{s,j} + Q_{i,j}) + \sum_{k=1}^{cr} (P_r + m), \tag{A19}$$

where cn is the number of pixels that are both adjacent to the channel and that have a flow direction into the channel, n is the number of layers in a soil column, and cr is the number of pixels within the channel.

Appendix B: Evapotranspiration Recovery Function Description

B1. Background

[59] Successional changes in forest transpiration are generally consistent with changes in forest Leaf Area Index (LAI), sapwood basal area, and net primary production (NPP) [*Watson et al.*, 1999; *Zimmermann et al.*, 2000]. *Ryan et al.*, [1997] found that forest LAI increases initially after disturbance, reaches a maximum in young stands, and thereafter decreases. *Moore et al.* [2004] found that young Douglas-fir forests in the Pacific Northwest have a higher sapwood basal area and use nearly three times as much water during the growing season as old-growth forests. *Acker et al.* [2002] found that the NPP of young stands in the Pacific Northwest is larger than the NPP of mature and old stands (Figure B1). Furthermore, several experimental studies found that the streamflow in managed forests is reduced to below old-growth values due to rapidly transpiring young vegetation [*Bond et al.*, 2008; *Hicks et al.*, 1991]. Finally, *Yang et al.* [2005] examined conifer development in 153 stands in the Pacific Northwest using interpretation of historic aerial photographs from 1959 to 1997 and found that coniferous forests regenerate quickly and reach closed canopy (defined as >70% tree cover) approximately 50 years after disturbance.

B2. Evapotranspiration Recovery Function

[60] Based on these findings, the ET function given in equation (A12) is modified to account for the (1) reduction in ET due to clearcut, (2) ET recovery during regrowth, (3) high transpiration demands of young forest, and (4) return to old-growth ET values within 50 years. Thus

$$ET_i = f_{TP}(t_d) \times W_{E,i} \times PET \times \left\{1 - \exp\left[-c_{ET} \times \left(s_i / s_i^{\max}\right)\right]\right\} \quad i = 1, 2, \ldots, n, \tag{B1}$$

where

$$f_{TP}(t_d) = f_{YF}(t_d) \times \{(1 - r_{ET}) \times [1 - \exp(-t_d / r_T)] + r_{ET}\} \tag{B2}$$

and

$$\text{for } (25 \le t_d \le 45 \text{ yrs } \& \; t_d \in \text{ Jun} - \text{Sept}) \quad f_{YF}(t_d) = \frac{\Omega}{\{(1 - r_{ET}) \times [1 - \exp(-t_d / r_T)] + r_{ET}\}} \quad \text{else} \quad f_{YF}(t_d) = 1, \tag{B3}$$

where $f_{TP}(t_d)$ is the ET recovery function, t_d is time in days after disturbance, r_{ET} is the residual ET immediately after clearcut, r_T is an ET recovery shape factor, and Ω is the percentage increase in transpiration of young stands over

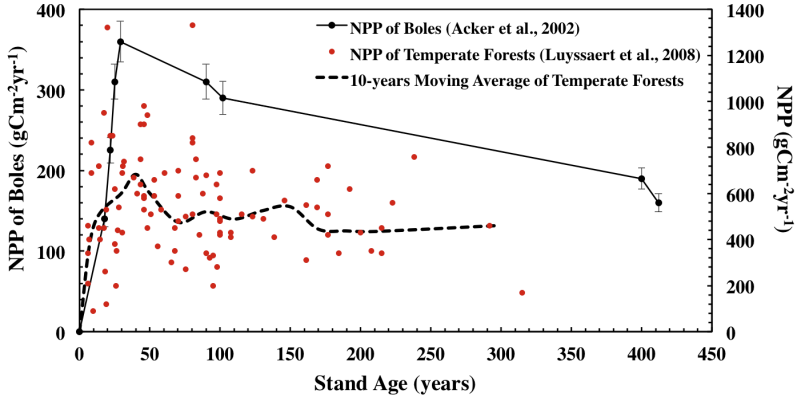

Figure B1. Changes in net primary production (NPP) of temperate forests (red dots are individual forest stands sampled throughout the world; dashed black line is a 10 year moving average) [*Luyssaert et al.*, 2008], and NPP of boles for Pacific Northwest coniferous forests (black circles and solid black line) as a function of stand age (i.e., time after stand-replacing disturbance) [*Acker et al.*, 2002].

Table B1. Model Parameters Values Used to Simulate the Hydrologic Processes of WS10 in the H.J. Andrews Experimental Forest

Parameters	Definition	Value	References
Soil texture	dominant soil texture	loam[a]	*Ranken* [1974]
θ_i^{fc}	field capacity in layer *i*	0.27	*Clapp and Hornberger* [1978]
ϕ_i	porosity in layer *i*	0.463	*Clapp and Hornberger* [1978]
θ_i^w	wilting point in layer *i*	0.117	*Clapp and Hornberger* [1978]
	Preharvest Calibrated Model Parameters		
Δz_1	soil surface layer (layer 1) thickness (mm)	300	calibrated
Δz_2	first intermediate soil layer (layer 2) thickness (mm)	750	calibrated
Δz_3	second intermediate soil layer (layer 3) thickness (mm)	750	calibrated
Δz_4	deep soil layer (layer 4) thickness (mm)	200	calibrated
Ks	surface saturated hydraulic conductivity (mm day^{-1})	950	calibrated
f_v	vertical decay rate of *Ks* (1/m)	1.3	calibrated
f_l	lateral decay rate of *Ks* (1/m)	1.55	calibrated
d_r	deepest layer in which water extraction is possible	3	*Santantonio et al.* [1977]
$W_{E,\ \mathrm{deep}}$	fraction of water uptake from the deep layers during droughts	0.2	calibrated
c_{ET}	ET *s*hape factor	5	calibrated
K_{PET}	potential evapotranspiration calibration parameter	2	calibrated
α	degree-day factor for melt (mm °C^{-1} day^{-1})	5	calibrated
T_{th}	threshold temperature (°C)	−1	calibrated
T_m	melting temperature (°C)	2	calibrated
σ	rain on snow parameter	0.5	calibrated
Che	Chezy "like" coefficient (1/day)	540,000	calibrated
	Postharvest Calibrated Model Parameters		
r_{ET}	residual evapotranspiration fraction after clearcut	0.3	calibrated
r_T	transpiration recovery shape factor	3000	calibrated
Ω	percentage increase in daily transpiration due to young vigorous forest (%)	10	calibrated

[a]Soil texture in WS10 range from gravelly, silty clay loam to very gravelly clay loam [*Ranken*, 1974].

old-growth during the growing season (assumed here between June and September). The function $f_{YF}(t_d)$ accounts for the increase in ET of young stands over old-growth.

[61] The ET recovery function $f_{TP}(t_d)$ is a modified Chapman-Richards growth function [*Hunt*, 1982; *Ratkowsky*, 1990; *Richards*, 1959] that accounts for the higher transpiration rate of young vigorous stands over old-growth [*Bond et al.*, 2008; *Jones and Post*, 2004]. Specifically, $f_{TP}(t_d)$ increases exponentially (from a clearcut value of $f_{TP}(t_d = 0) = r_{ET}$) and asymptotes to old-growth values within 50 years (i.e., $f_{TP}(t_d = 50\ \mathrm{yrs}) = 1$). This ET recovery function (B2) is an initial attempt to capture the complex successional dynamics associated with canopy recovery. This function has been widely used in studies of trees and stand growth (e.g., at the H.J. Andrews, the Coweeta, and the Hubbard Brook Experimental Forests) [*Bosch and Von Gadow*, 1990; *Christina et al.*, 2011; *Duan*, 1996; *Janisch and Harmon*, 2002; *Khamis et al.*, 2005; *Waichler et al.*, 2005; *Zeide*, 1993, among others]. *Waichler et al.* [2005] used the Chapman-Richards growth function to capture canopy recovery in three watersheds within H.J. Andrews. *Yang et al.* [2005] used the Chapman-Richards growth function to simulate the recovery of shrubs, hardwood trees, conifer trees, and mixed trees successional postdisturbance dynamics.

[62] Calibration of the ET recovery function parameters is conducted as follows: Ω is calibrated to capture the observed 1975–2008 annual, seasonal, and monthly streamflow. r_{ET} is calibrated based on the annual P and Q_T record at WS10 immediately after clearcut and yields a value of 30% (Table B1), which is well within the range of observed values in forests across the United States and the Pacific Northwest [*Spittlehouse*, 2006; *Stednick*, 1996; *Stoy et al.*, 2006; *Winkler et al.*, 2010]. For example, a number of studies in the Pacific Northwest, including H.J. Andrews, have found that the initial ET after clearcut ranged from 280 to 550 mm (30% to 55% of preclearcut ET) [*Bosch and Hewlett*, 1982; *Hibbert*, 1966; *Stednick*, 1996].

[63] **Acknowledgments.** The information in this document has been funded in part by the U.S. Environmental Protection Agency. It has been subjected to the Agency's peer and administrative review, and it has been approved for publication as an EPA document. Mention of trade names or commercial products does not constitute endorsement or recommendation for use. This research was additionally supported in part by the following NSF Grants 0439620, 0436118, and 0922100. We thank Sherri Johnson, Barbara Bond, Suzanne Remillard, Theresa Valentine, and Don Henshaw for invaluable assistance in accessing and interpreting various H.J. Andrews LTER data sets used in this study. Data for streamflow, stream chemistry and climate were provided by the H.J. Andrews Experimental Forest research program, funded by the National Science Foundation's Long-Term Ecological Research Program (DEB 08-23380), U.S. Forest Service Pacific Northwest Research Station, and OR State University.

References

Acker, S., C. Halpern, M. Harmon, and C. Dyrness (2002), Trends in bole biomass accumulation, net primary production and tree mortality in Pseudotsuga menziesii forests of contrasting age, *Tree Physiol.*, *22*(2–3), 213.

Beckers, J., B. Smerdon, T. Redding, A. Anderson, R. Pike, and A. T. Werner (2009), Hydrologic models for forest management applications: Part 1: Model selection, *Watershed Manage. Bull.*, *13*(1), 35–44.

Beschta, R. L. (1978), Long-term patterns of sediment production following road construction and logging in the Oregon Coast Range, *Water Resour. Res.*, *14*(6), 1011–1016, doi:1010.1029/WR1014i1006p01011.

Beschta, R., M. Pyles, A. Skaugset, and C. Surfleet (2000), Peakflow responses to forest practices in the western Cascades of Oregon, USA, *J. Hydrol.*, *233*(1–4), 102–120.

Beven, K., and M. Kirkby (1979), A physically based, variable contributing area model of basin hydrology, *Hydrol. Sci. Bull.*, *24*(1), 43–69.

Bond, B. J., F. C. Meinzer, and J. R. Brooks (2008), How trees influence the hydrological cycle in forest ecosystems, in *Hydroecology and Ecohydrology: Past, Present and Future*, edited by P. Wood, pp. 7–28, John Wiley, Chichester, U. K.

Bond-Lamberty, B., S. T. Gower, D. E. Ahl, and P. E. Thornton (2005), Reimplementation of the Biome-BGC model to simulate successional change, *Tree Physiol.*, *25*(4), 413.

Bosch, J., and J. Hewlett (1982), A review of catchment experiments to determine the effect of vegetation changes on water yield and evapotranspiration, *J. Hydrol.*, *55*(1–4), 3–23.

Bosch, J., and K. Von Gadow (1990), Regulating afforestation for water conservation in South Africa, *South African For. J.*, *153*(1), 41–54.

Bowling, L. C., P. Storck, and D. P. Lettenmaier (2000), Hydrologic effects of logging in western Washington, United States, *Water Resour. Res.*, *36*(11), 3223–3240, doi:10.1029/2000WR900138.

Brooks, J. R., F. C. Meinzer, J. M. Warren, J. C. Domec, and R. Coulombe (2006), Hydraulic redistribution in a Douglas-fir forest: Lessons from system manipulations, *Plant Cell Environ.*, *29*(1), 138–150.

Christina, M., J. P. Laclau, J. Goncalves, C. Jourdan, Y. Nouvellon, and J. P. Bouillet (2011), Almost symmetrical vertical growth rates above and below ground in one of the world's most productive forests, *Ecosphere*, *2*(3), article 27, doi:10.1890/ES10-00158.1.

Clapp, R. B., and G. M. Hornberger (1978), Empirical equations for some soil hydraulic properties, *Water Resour. Res.*, *14*(4), 601–604, doi:610.1029/WR1014i1004p00601.

Daly, C., and W. McKee (2011), Meteorological data from benchmark stations at the Andrews Experimental Forest. Long-Term Ecological Research. Forest Science Data Bank, Corvallis, OR. [Database]. Available: http://andrewsforest.oregonstate.edu/data/abstract.cfm?dbcode=MS001 (16 July 2011).

Davies, J., and C. Allen (1973), Equilibrium, potential and actual evaporation from cropped surfaces in southern Ontario, *J. Appl. Meteorol.*, *12*(4), 649–657.

Dingman, S. (1994), *Physical Hydrology*, Prentice Hall, Upper Saddle River, NJ.

Duan, J. (1996), A coupled hydrologic-geomorphic model for evaluating effects of vegetation change on watersheds, Ph.D. Dissertation, 133 pp., Oregon State University, Corvallis, OR.

Dyrness, C. (1973), Early stages of plant succession following logging and burning in the western Cascades of Oregon, *Ecology*, *54*(1), 57–69.

Federer, C. A. (1979), A soil-plant-atmosphere model for transpiration and availability of soil water, *Water Resour. Res.*, *15*(3), 555–562, doi:510.1029/WR1015i1003p00555.

Federer, C. A. (1982), Transpirational supply and demand: Plant, soil, and atmospheric effects evaluated by simulation, *Water Resour. Res.*, *18*(2), 355–362, doi:310.1029/WR1018i1002p00355.

Fredriksen, R. (1975), Nitrogen, phosphorus and particulate matter budgets of five coniferous forest ecosystems in the western Cascades Range, Oregon, Ph.D. Thesis, 71 pp, Oregon State University, Corvallis.

Freeman, T. (1991), Calculating catchment area with divergent flow based on a regular grid, *Comput. Geosci.*, *17*(3), 413–422.

Gale, M. R., and D. F. Grigal (1987), Vertical root distributions of northern tree species in relation to successional status, *Can. J. For. Res.*, *17*(8), 829–834.

Garrick, M., C. Cunnane, and J. Nash (1978), A criterion of efficiency for rainfall-runoff models, *J. Hydrol.*, *36*(3–4), 375–381.

Gholz, H. L., G. M. Hawk, A. Campbell, K. Cromack Jr., and A. T. Brown (1985), Early vegetation recovery and element cycles on a clear-cut watershed in western Oregon, *Can. J. For. Res.*, *15*(2), 400–409.

Golding, D. L. (1987), Changes in streamflow peaks following timber harvest of a coastal British Columbia watershed, paper presented at Forest Hydrology and Watershed Management, IAHS, Vancouver.

Grant, G., S. Lewis, F. Swanson, J. Cissel, and J. McDonnell (2008), Effects of forest practices on peak flows and consequent channel response: a state-of-science report for western Oregon and Washington, General Technical Report PNW-GTR-760, Portland, OR: USDA Forest Service, Pacific Northwest Research Station, 76.

Grier, C., and R. Logan (1977), Old-growth Pseudotsuga menziesii communities of a western Oregon watershed: biomass distribution and production budgets, *Ecol. Mono.*, *47*(4), 373–400.

Hacke, U., J. Sperry, B. Ewers, D. Ellsworth, K. Schäfer, and R. Oren (2000), Influence of soil porosity on water use in Pinus taeda, *Oecologia*, *124*(4), 495–505.

Hamon, W. (1963), Computation of direct runoff amounts from storm rainfall, *Int. Assoc. Sci. Hydrol. Symp. Surf. Waters*, *3*, 52–62.

Harmon, M. E., W. K. Ferrell, and J. F. Franklin (1990), Effects on carbon storage of conversion of old-growth forests to young forests, *Science*, *247*(4943), 699–701.

Harr, R. (1981), Some characteristics and consequences of snowmelt during rainfall in western Oregon, *J. Hydrol.*, *53*(3–4), 277–304.

Harr, R., and F. M. McCorison (1979), Initial effects of clearcut logging on size and timing of peak flows in a small watershed in western Oregon, *Water Resour. Res.*, *15*(1), 90–94, doi:10.1029/WR1015i1001p00090.

Harr, R., R. Fredriksen, and J. Rothacher (1979), Changes in streamflow following timber harvest in southwestern Oregon, Research Paper PNW-RP-249, Portland, OR: U.S. Department of Agriculture, Forest Service, Pacific Northwest Research Station, 22.

Harr, R., A. Levno, and R. Mersereau (1982), Streamflow changes after logging 130-year-old Douglas-fir in two small watersheds, *Water Resour. Res.*, *18*(3), 637–644, doi:610.1029/WR1018i1003p00637.

Hibbert, A. (1966), Forest treatment effects on water yield, in *Proceedings of a National Science Foundation Advanced Science Seminar, International Symposium on Forest Hydrology*, edited by W. E. Sopper and H. W. Lull, pp. 527–543, Pergamon, New York.

Hicks, B., R. Beschta, and R. Harr (1991), Long-term changes in streamflow following logging in western Oregon and associated fisheries implications, *Water Resour. Bull.*, *27*(2), 217–226.

Hood, E., M. N. Gooseff, and S. L. Johnson (2006), Changes in the character of stream water dissolved organic carbon during flushing in three small watersheds, Oregon, *J. Geophys. Res.*, *111*, G01007, doi:10.1029/2005JG000082.

Huang, J., S. Lacey, and P. Ryan (1996), Impact of forest harvesting on the hydraulic properties of surface soil, *Soil Science*, *161*(2), 79.

Hunt, R. (1982), *Plant Growth Curves: The Functional Approach to Plant Growth Analysis*, 248 pp., Edward Arnold, London.

Jackson, R., J. Canadell, J. Ehleringer, H. Mooney, O. Sala, and E. Schulze (1996), A global analysis of root distributions for terrestrial biomes, *Oecologia*, *108*(3), 389–411.

Janisch, J., and M. Harmon (2002), Successional changes in live and dead wood carbon stores: implications for net ecosystem productivity, *Tree Physiol.*, *22*(2–3), 77.

Johnson, S., and J. Rothacher (2009), Stream discharge in gaged watersheds at the Andrews Experimental Forest. Long-Term Ecological Research. Forest Science Data Bank, Corvallis, OR. [Database]. Available: http://andrewsforest.oregonstate.edu/data/abstract.cfm?dbcode=HF004 (16 July 2011).

Jones, J. A. (2000), Hydrologic processes and peak discharge response to forest removal, regrowth, and roads in 10 small experimental basins, western Cascades, Oregon, *Water Resour. Res.*, *36*(9), 2621–2642, doi:2610.1029/2000WR900105.

Jones, J. A., and G. E. Grant (1996), Peak flow responses to clear-cutting and roads in small and large basins, western Cascades, Oregon, *Water Resour. Res.*, *32*(4), 959–974, doi:10.1029/95WR03493.

Jones, J. A., and D. A. Post (2004), Seasonal and successional streamflow response to forest cutting and regrowth in the northwest and eastern United States, *Water Resour. Res.*, *40*(5), W05203, doi:10.1029/2003WR002952.

Jordan, T., D. Correll, and D. Weller (1993), Nutrient interception by a riparian forest receiving inputs from adjacent cropland, *J. Environ. Qual.*, *22*(3), 467.

Keppeler, E. T., and R. R. Ziemer (1990), Logging effects on streamflow: water yield and summer low flows at Caspar Creek in northwestern California, *Water Resour. Res.*, *26*(7), 1669–1679, doi:10.1029/WR026i007p01669.

Khamis, A., Z. Ismail, K. Haron, and A. T. Mohammed (2005), Nonlinear growth models for modeling oil palm yield growth, *J. Math. Stat.*, *1*(3), 225–233.

Kirchner, J. (2003), A double paradox in catchment hydrology and geochemistry, *Hydrol. Processes*, *17*(4), 871–874.

Legates, D. R., and G. J. McCabe Jr. (1999), Evaluating the use of "goodness-of-fit" measures in hydrologic and hydroclimatic model validation, *Water Resour. Res.*, *35*(1), 233–241, doi:10.1029/1998WR900018.

Lowrance, R., L. Altier, J. Newbold, R. Schnabel, P. Groffman, J. Denver, D. Correll, J. Gilliam, J. Robinson, and R. Brinsfield (1997), Water quality functions of riparian forest buffers in Chesapeake Bay watersheds, *Environ. Manage.*, *21*(5), 687–712.

Luce, C., and B. Wemple (2001), Introduction to special issue on hydrologic and geomorphic effects of forest roads, *Earth Surf. Processes Landforms*, *26*(2), 111–113.

Luyssaert, S., E. Schulze, A. Borner, A. Knohl, D. Hessenmoller, B. Law, P. Ciais, and J. Grace (2008), Old-growth forests as global carbon sinks, *Nature*, *455*(7210), 213–215.

McGuire, K., M. Weiler, and J. McDonnell (2007), Integrating tracer experiments with modeling to assess runoff processes and water transit times, *Adv. Water Resour.*, *30*(4), 824–837.

McKane, R., E. Rastetter, G. Shaver, K. Nadelhoffer, A. Giblin, J. Laundre, and F. Chapin III (1997), Climatic effects on tundra carbon storage inferred from experimental data and a model, *Ecology*, *78*(4), 1170–1187.

Moore, G., B. Bond, J. Jones, N. Phillips, and F. Meinzer (2004), Structural and compositional controls on transpiration in 40-and 450-year-old riparian forests in western Oregon, USA, *Tree Physiol.*, *24*(5), 481.

Moore, R., and S. Wondzell (2005), Physical hydrology in the Pacific Northwest and the effects of forest harvesting: A review, *J. Am. Water Resour. Assoc.*, *41*, 753–784.

Nash, J., and J. Sutcliffe (1970), River flow forecasting through conceptual models part I—A discussion of principles, *J. Hydrol.*, *10*(3), 282–290.

Purser, M. D., and T. W. Cundy (1992), Changes in soil physical properties due to cable yarding and their hydrologic implications, *West. J. Appl. For.*, *7*(2), 36–39.

Quinn, P., K. Beven, P. Chevallier, and O. Planchon (1991), Prediction of hillslope flow paths for distributed hydrological modelling using digital terrain models, *Hydrol. Processes*, *5*(1), 59–79.

Rango, A., and J. Martinec (1995), Revisiting the degree-day method for snowmelt computations, *Water Resour. Bull.*, *31*(4), 657–669.

Ranken, D. W. (1974), Hydrologic properties of soil and subsoil on a steep, forested slope, Master's thesis, 117 pp, Oregon State University, Corvallis.

Ratkowsky, D. (1990), *Handbook of Nonlinear Regression Models*, volume 107 of Statistics: Textbooks and Monographs, Marcel Dekker, New York.

Richards, F. (1959), A flexible growth function for empirical use, *J. Exp. Botany*, *10*(29), 290–300.

Rothacher, J. (1965), Streamflow from small watersheds on the western slope of the Cascade Range of Oregon, *Water Resour. Res.*, *1*, 125–134, doi:110.1029/WR1001i1001p00125.

Rothacher, J. (1970), Increases in water yield following clear-cut logging in the Pacific Northwest, *Water Resour. Res.*, *6*(2), 653–658, doi:610.1029/WR1006i1002p00653.

Ryan, M., D. Binkley, and J. H. Fownes (1997), Age-related decline in forest productivity: pattern and process, *Adv. Ecol. Res.*, *27*, 213–262.

Sahin, V., and M. Hall (1996), The effects of afforestation and deforestation on water yields, *J. Hydrol.*, *178*(1–4), 293–309.

Santantonio, D., R. Hermann, and W. Overton (1977), Root biomass studies in forest ecosystems, Pedobiologia, Bd. 17, S. 1–31, Paper 957, Forest Research Laboratory, School of Forestry Oregon State University, Corvallis, Oregon.

Sayama, T., and J. McDonnell (2009), A new time-space accounting scheme to predict stream water residence time and hydrograph source components at the watershed scale, *Water Resour. Res.*, *45*, W07401, doi:10.1029/2008WR007549.

Sidle, R. C., S. Noguchi, Y. Tsuboyama, and K. Laursen (2001), A conceptual model of preferential flow systems in forested hillslopes: Evidence of self organization, *Hydrol. Processes*, *15*(10), 1675–1692.

Sollins, P., and F. M. McCorison (1981), Nitrogen and carbon solution chemistry of an old growth coniferous forest watershed before and after cutting, *Water Resour. Res.*, *17*(5), 1409–1418, doi:1410.1029/WR1017i1005p01409.

Sollins, P., K. Cromack Jr., F. Mc Corison, R. Waring, and R. Harr (1981), Changes in nitrogen cycling at an old-growth Douglas-fir site after disturbance, *J. Environ. Qual.*, *10*(1), 37.

Spittlehouse, D. (2006), Annual water balance of high elevation forests and clearcuts, in Proceedings of the 27th Conference on Agricultural and Forest Meteorology, San Diego, CA, American Meteorological Society, Boston, MA, 7 pp.

Spittlehouse, D. L., and T. A. Black (1981), A growing season water balance model applied to two Douglas fir stands, *Water Resour. Res.*, *17*(6), 1651–1656, doi:10.1029/WR017i006p01651.

Startsev, A., and D. McNabb (2000), Effects of skidding on forest soil infiltration in west-central Alberta, *Can. J. Soil Sci.*, *80*(4), 617–624.

Stednick, J. (1996), Monitoring the effects of timber harvest on annual water yield, *J. Hydrol.*, *176*(1–4), 79–95.

Stoy, P. C., G. G. Katul, M. Siqueira, J. Y. Juang, K. A. Novick, H. R. Mccarthy, A. C. Oishi, J. M. Uebelherr, H. S. Kim, and R. Oren (2006), Separating the effects of climate and vegetation on evapotranspiration along a successional chronosequence in the southeastern US, *Global Change Biol.*, *12*(11), 2115–2135.

Swanson, F., and C. Dyrness (1975), Impact of clear-cutting and road construction on soil erosion by landslides in the western Cascade Range, Oregon, *Geology*, *3*(7), 393.

Swanston, D., and F. Swanson (1976), Timber harvesting, mass erosion, and steepland forest geomorphology in the Pacific Northwest, in *Geomorphology and Engineering*, edited by D. R. Coates, pp. 199–221, Dowden, Hutchinson, and Ross, Stroudsburg, Pa.

Tachikawa, Y., G. Nagatani, and K. Takara (2004), Development of stage discharge relationship equation incorporating saturated-unsaturated flow mechanism, *Annu. J. Hydraul. Eng. Jpn. Soc. Civil Eng.*, *48*, 7–12.

Tague, C., and L. Band (2000), Simulating the impact of road construction and forest harvesting on hydrologic response, *Earth Surf. Processes Landforms*, *26*(2), 135–151.

Valentine, T., and G. Lienkaemper (2005), 30 meter digital elevation model (DEM) clipped to the Andrews Experimental Forest. Long-Term Ecological Research. Forest Science Data Bank, Corvallis, OR. [Database]. Available: http://andrewsforest.oregonstate.edu/data/abstract.cfm?dbcode=GI002 (16 July 2011).

Vanderbilt, K., K. Lajtha, and F. Swanson (2003), Biogeochemistry of unpolluted forested watersheds in the Oregon Cascades: Temporal patterns of precipitation and stream nitrogen fluxes, *Biogeochemistry*, *62*(1), 87–117.

Van Verseveld, W. J., J. J. McDonnell, and K. Lajtha (2008), A mechanistic assessment of nutrient flushing at the catchment scale, *J. Hydrol.*, *358*(3–4), 268–287.

Waichler, S. R., B. C. Wemple, and M. S. Wigmosta (2005), Simulation of water balance and forest treatment effects at the HJ Andrews Experimental Forest, *Hydrol. Processes*, *19*(16), 3177–3199.

Warren, J., F. Meinzer, J. Brooks, and J. Domec (2005), Vertical stratification of soil water storage and release dynamics in Pacific Northwest coniferous forests, *Agr. For. Meteorol.*, *130*(1–2), 39–58.

Watson, F., R. Vertessy, and R. Grayson (1999), Large-scale modelling of forest hydrological processes and their long-term effect on water yield, *Hydrol. Processes*, *13*(5), 689–700.

Wemple, B. C., and J. A. Jones (2003), Runoff production on forest roads in a steep, mountain catchment, *Water Resour. Res.*, *39*(8), 1220, doi:10.1029/2002WR001744.

Wemple, B. C., F. J. Swanson, and J. A. Jones (2001), Forest roads and geomorphic process interactions, Cascade Range, Oregon, *Earth Surf. Processes Landforms*, *26*(2), 191–204.

Whitaker, A., Y. Alila, J. Beckers, and D. Toews (2002), Evaluating peak flow sensitivity to clear-cutting in different elevation bands of a snowmelt-dominated mountainous catchment, *Water Resour. Res.*, *38*(9), 1172, doi:10.1029/2001WR000514.

Wigmosta, M. S., and W. A. Perkins (2001), Simulating the effects of forest roads on watershed hydrology, *Land Use Watersheds Human Influence Hydrol. Geomorphol. Urban For. Areas*, *2*, 127–143.

Wigmosta, M. S., L. W. Vail, and D. P. Lettenmaier (1994), A distributed hydrology-vegetation model for complex terrain, *Water Resour. Res.*, *30*(6), 1665–1680, doi:1610.1029/1694WR00436.

Willmott, C. J. (1981), On the validation of models, *Phys. Geograph.*, *2*(2), 184–194.

Winkler, R. D., R. D. Moore, T. Redding, D. Spittlehouse, B. Smerdon, and D. Carlyle-Moses (2010), The effects of forest disturbance on hydrologic processes and watershed response, in Compendium of Forest Hydrology and Geomorphology in British Columbia, edited by R. G. Pike et al., pp. 179–212, B. C. Minist. of For. and Range Res. Branch, Victoria, B. C., Canada.

Yang, Z., W. Cohen, and M. Harmon (2005), Modeling early forest succession following clear-cutting in western Oregon, *Can. J. For. Res.*, *35*(8), 1889–1900.

Zeide, B. (1993), Analysis of growth equations, *For. Sci.*, *39*(3), 594–616.

Zimmermann, R., E. D. Schulze, C. Wirth, E. E. Schulze, K. C. Mcdonald, N. N. Vygodskaya, and W. Ziegler (2000), Canopy transpiration in a chronosequence of Central Siberian pine forests, *Global Change Biol.*, *6*(1), 25–37.

A. Abdelnour, Department of Civil and Environmental Engineering, Georgia Institute of Technology, 200 Bobby Dodd Way, Atlanta, GA 30313, USA. (alexabdelnour@gatech.edu)

R. McKane, U.S. Environmental Protection Agency, 200 SW 35th Street, Corvallis, OR 97333, USA.

F. Pan, Department of Geography, University of North Texas, 1704 W. Mulberry, Denton, TX 76203, USA.

M. Stieglitz, Department of Civil and Environmental Engineering, School of Earth Atmospheric Sciences, Georgia Institute of Technology, 200 Bobby Dodd Way, Atlanta, GA 30313, USA.